



**Article title:** The closure of the Vardar ocean (the western domain of the northern Neotethys) from early Middle Jurassic to Paleocene time, based on surface geology of eastern Pelagonia and the Vardar zone, biostratigraphy, and seismic-tomographic images of the mantle below the Central Hellenides

**Authors:** Rudolph Scherreiks[1], Marcelle Boudagher-Fadel[2]

**Affiliations:** Geologische Staatssammlung of the Bayerische Staatssammlung für Palaeontologie und Geologie, Germany[1], Professorial Research Fellow, Office of the Vice-Provost (Research), University College London, UK[2]

**Orcid ids:** 0000-0002-2777-1476[1], 0000-0002-2339-2444[2]

**Contact e-mail:** m.fadel@ucl.ac.uk

**License information:** This is an open access article distributed under the terms of the Creative Commons Attribution License (CC BY) 4.0 <https://creativecommons.org/licenses/by/4.0/>, which permits unrestricted use, distribution and reproduction in any medium, provided the original author and source are credited.

**Preprint statement:** This article is a preprint and has not been peer-reviewed, under consideration and submitted to UCL Open: Environment Preprint for open peer review.

**Funder:** N/A

**DOI:** 10.14324/111.444/000078.v2

**Preprint first posted online:** 08 July 2021

**Keywords:** Adria, Pelagonia, Vardar, subduction and obduction, ocean lithosphere, tectono-stratigraphy, biostratigraphy, tomographic images, ophiolite, carbonate platforms, The Environment, Climate, Built environment

1 **The closure of the Vardar ocean (the western domain of the**  
2 **northern Neotethys) from early Middle Jurassic to Paleocene time,**  
3 **based on surface geology of eastern Pelagonia and the Vardar**  
4 **zone, biostratigraphy, and seismic-tomographic images of the**  
5 **mantle below the Central Hellenides**

6  
7 Rudolph Scherreiks<sup>1</sup> Marcelle BouDagher-Fadel<sup>2</sup>

8  
9 <sup>1</sup>Geologische Staatssammlung of the Bayerische Staatssammlung für  
10 Palaeontologie und Geologie, Luisenstr. 37, 80333 Munich, Germany

11 <sup>2</sup>University College London, Office of the Vice-Provost (Research), 2  
12 Taviton Street, WC 1 H OBT, London, UK

13  
14 **Abstract**

15 Seismic tomographic images of the mantle below the Hellenides indicate  
16 that the Vardar ocean probably had a composite width of over 3000  
17 kilometres. From surface geology we know that this ocean was initially  
18 located between two passive margins: Pelagonian Adria in the west and  
19 Serbo-Macedonian-Eurasia in the east. Pelagonia was covered by a  
20 carbonate platform that accumulated, during Late Triassic to Early  
21 Cretaceous time, where highly diversified carbonate sedimentary  
22 environments evolved and reacted to the adjacent, converging Vardar  
23 ocean plate. We conceive that on the east side of the Vardar ocean, a  
24 Cretaceous carbonate platform evolved from Aptian to Maastrichtian  
25 time in the forearc basin of the Vardar supra-subduction volcanic arc  
26 complex.

27 The closure of the Vardar ocean occurred in one episode of ophiolite  
28 obduction and in two episodes of intra-oceanic subduction.

29 1. During Middle Jurassic time a 1200-kilometre slab of west Vardar  
30 lithosphere subducted beneath the supra-subduction, "Eohellenic", arc,  
31 while a 200-kilometre-wide slab obducted onto Pelagonia between  
32 Callovian and Valanginian time.

33 2. During Late Jurassic through Cretaceous time a 1700-kilometre-wide  
34 slab subducted beneath the evolving east Vardar-zone arc-complex.  
35 Pelagonia, the trailing edge of the subducting east-Vardar ocean slab,  
36 crashed and underthrust the Vardar arc complex during Paleocene time  
37 and ultimately crashed with Serbo-Macedonia. Since late Early Jurassic  
38 time, the Hellenides have moved about 3000 kilometres toward the  
39 northeast while the Atlantic Ocean spread.

41 **Key Words** Adria, Pelagonia, Vardar, subduction, obduction, tectono-  
42 stratigraphy, biostratigraphy, tomographic images, ophiolite, carbonate  
43 platforms, ocean lithosphere

## 44 **Introduction**

45 Relicts of oceanic lithosphere can be traced from the Dinarides through  
46 the Hellenides and Taurides. They bear witness to the once extensive  
47 northern Neotethys ocean (Fig 1) (Stampfli and Borel 2004; Schmid et  
48 al. 2008; Schmid et al. 2020). In this contribution, we shed new light on  
49 the palaeogeography and subduction of the Vardar branch of the  
50 Neotethys from Early Jurassic through early Palaeocene time, which we  
51 have gained from our research on the tectono-stratigraphy of the Vardar  
52 zone of Greek Macedonia and from the eastern Pelagonian zone of  
53 Northern Evvoia and the Northern Sporades (Fig.1). This surface  
54 geology is aligned with seismic tomographic images that depict two  
55 perturbations in the mantle below the central Hellenides, that we  
56 interpret as two slabs of Vardar ocean lithosphere, which sank into the  
57 mantle during two episodes of subduction. We also show that two  
58 carbonate platforms evolved, one on each side of the Vardar ocean and  
59 they reacted to and were tectonically involved with the obduction,  
60 subduction and ultimate closure of the Vardar ocean.

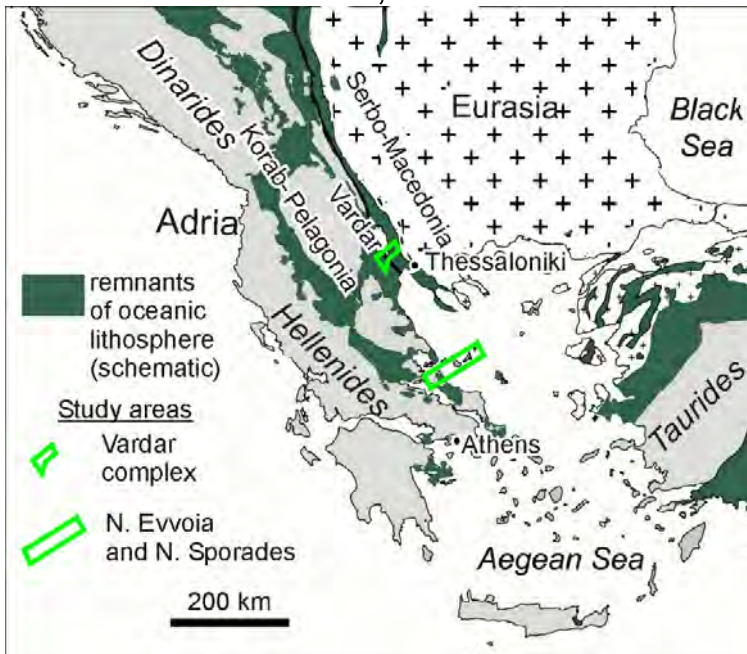
61 A time-lapse reconstruction is presented of the convergence and  
62 subduction of the Vardar ocean from Early Jurassic through early  
63 Paleocene time. We give answers to questions concerning the original  
64 width of the Vardar ocean and how closure took place and ended with  
65 Pelagonia's collision with the Vardar Island-arc-complex and the  
66 detachment and subsidence of the Vardar ocean slabs into the mantle.

## 67 **Geological Background**

### 68 ***The Neotethys, Vardar zone and some nomenclature***

69 In palaeogeographic reconstructions of the evolution of the Palaeotethys  
70 and Neotethys, Stampfli and Borel (2004) show that the northern  
71 Neotethys ocean opened as the Palaeotethys closed (fig. 2a): the Maliac  
72 ocean is a remnant of the Paleotethys, which, through intra-oceanic  
73 subduction, becomes overthrust by the Vardar ocean at the western end  
74 of the northern Neotethys. Alternatively, the Vardar ocean can simply be  
75 envisioned to have opened as a western continuation of the Neotethys  
76 (Sengor and Natal'in (1996) in Hafkingscheid (2004)).

77 In an enlightening palaeogeographic reconstruction of the Mid-Late  
78 Jurassic Vardar ocean, shown in Schmid et al. (2020) the Vardar ocean



79  
80 Fig. 1 (see figure captions)

81  
82 has two eastward dipping, Intra-oceanic subduction zones and an arc  
83 complex (Fig.2b). This model implies that the Vardar ocean existed from  
84 Early Mesozoic to Late Cretaceous time (in agreement with Sharp and  
85 Robertson 2006). Our research corroborates these plate-tectonic  
86 palaeogeographic interpretations which we have proceeded to  
87 investigate both spatially and temporally. Following Schmid et al. (2008)  
88 the present contribution supports the one-ocean concept, that the Vardar  
89 ophiolites were obducted westward over the Korab-Pelagonian zone of  
90 east Adria (Fig. 2b). For other models in which western Pelagonia had  
91 plate-tectonic involvement with an inferred Pindos ocean see Sharp and  
92 Robertson (2006). Our investigations, however, have been limited to  
93 eastern Pelagonia and the Vardar zone (Fig. 1).

94  
95  
96

### 97 *Nomenclature*

98 For nomenclatural orientation, “Vardar ocean” is the name of the  
99 western ocean domain of the northern Neotethys (Fig.2b). We agree

100

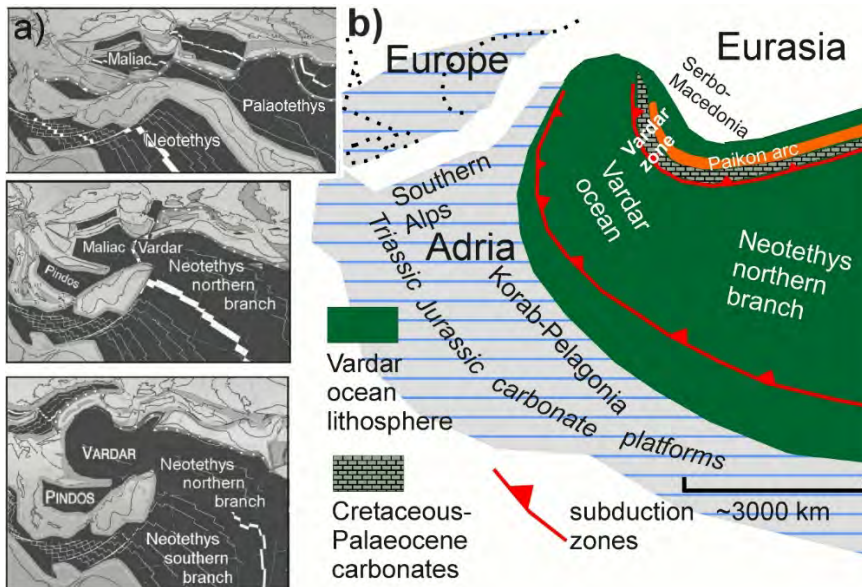


Fig. 2 (see figure captions)

101

102

103

104

105

106

107

108

109

110

111

112

113

114

115

116

117

118

119

120

121

122

123

124

125

126

127

128

129

130

with Schmid et al. (2020) that “Vardar zone” (Fig. 2b) is not synonymous with “Vardar ocean”. In our opinion, the Vardar zone is not the “root” of Vardar-derived thrust sheets, as has been often suggested (Zimmerman and Ross 1976; Brown and Robertson 2004; Froitzheim et al. 2014).

Quite the contrary, as will be shown, the “Vardar zone” is where the last slab of the Vardar ocean subducted (Scherreiks and BouDagher-Fadel 2020a and 2020b) and probably corresponds to the “Sava suture zone” (Ustaszewski et al. 2010; Schmid et al. 2020).

The names of geo-tectonic sub-divisions of the Vardar zone used herein are after Kockel (1979).

The “Vardar zone” corresponds to the northwest-southeast striking belt (Fig. 1) where remnants of island arc volcanic formations are found (Mercier, 1968; BeBien et al. 1994; Brown & Robertson 1994; Mercier and Vergely, 2002; Saccani et al. 2008; Sharp and Robertson 2006; Katrivanos 2013) and where easternmost Pelagonia is covered by Upper Cretaceous carbonates (Schmid et al. 2020).

We consider it important to use the term “ophiolite,” in the strict sense of the “Steinmann Trinity” (Bernoulli et al.), because there are oceanic formations in the study areas that are composed of basalt +/- radiolarite but are devoid of serpentinite and were derived from tectonic environments unrelated to obduction, which will be shown.

Furthermore, the term “mélange”, used herein, follows Hsü (1974) referring to tectonically produced polymictic fault-zone rocks as opposed to polymictic sedimentary deposits (see also Scherreiks 2000). The mélanges are associated with mylonitic S-C shear fabrics of subduction zones (Meneghini et al. 2009) like those found in the Vardar zone (Katrivanos et al. 2013).



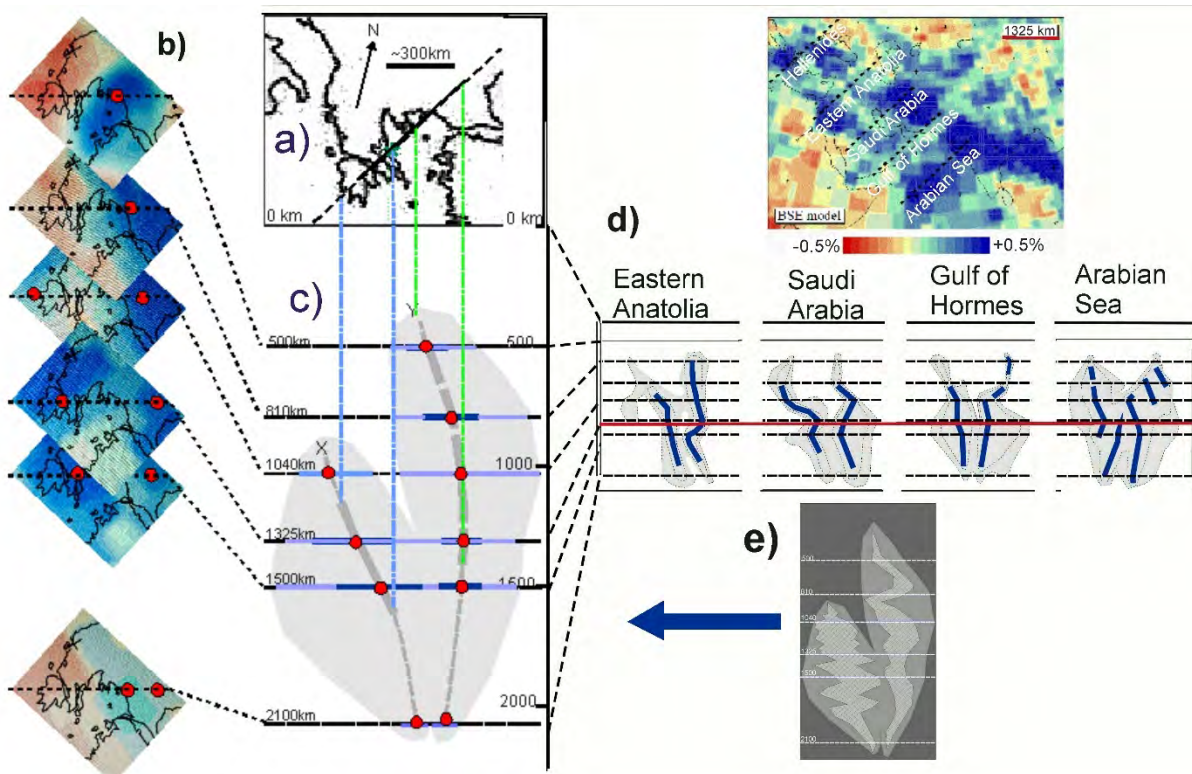


Fig. 3 (see figure captions)

### ***The carbonate platforms of Adria and the Vardar zone***

Following the afore said and our own research, Adria was the fundamental pedestal of a vast subsiding carbonate platform, of the marginal, foreland category (Kendall and Schlager 1981; Schlager 2000; Bosence 2005) that extended from the Alps (Fruth and Scherreiks 1982, Bosellini 1984) through Korab-Pelagonia and into the west Taurides (Flügel 1974,1983; Scherreiks 2000) (Fig. 1, Fig. 2b) and across the western Adria (BouDagher-Fadel and Bosence 2007). The platform evolved adjacent to the west side of the Vardar ocean during the Late Triassic through the Early Jurassic from a cyclically alternating supratidal to a peritidal domain (Scherreiks 2000; Bosence et al. 2009) and then responded with subsidence and episodes of upheaval as continental Adria and the Vardar ocean converged (Scherreiks et al. 2010, 2014, 2016). (Table 1a documents biostratigraphic data concerning the Pelagonian carbonate platform of Evvoia and the Northern Sporades, which will be referred to in the text.)

In the Vardar zone at the east side of the Vardar ocean (Fig. 2b) one finds the remnants of a carbonate platform that evolved during the Cretaceous, most probably on the forearc margin of the Vardar arc (Fig.2b) whose evolution terminated during the Paleocene (Mercier 1968; Mercier and Vergely 2002). The inevitable crash between Pelagonia and the Vardar zone (Fig.2b) was a collision between two

157 Cretaceous platforms (see Discussion). (Significant biostratigraphic data  
158 concerning carbonate platform of the Vardar zone are documented in  
159 Tables 1b and 1c and will referred to).

160

161 ***The Pelagonian carbonate platform and its involvement in the***  
162 ***demise of the Vardar ocean***

163 The Vardar ocean existed during the Middle to Late Triassic,  
164 substantiated by radiolarians and pillow basalt found in ophiolite  
165 occurrences in our study area in Evvoia (Danelian and Robertson 2001;  
166 Chiari and Marcucci 2003; Gingins and Schauner 2005; Gawlick et al.  
167 2008; Scherreiks et al. 2010; Chiari et al. 2012) (Table 1a11.1). Initially,  
168 the Late Triassic and Early Jurassic carbonate platform evolved from a  
169 cyclically alternating supratidal to peritidal domain (Scherreiks 2000;  
170 Bosence et al. 2009) and then began sinking, presumably responding  
171 with subsidence as Adria converged with the Vardar oceanic plate  
172 (Scherreiks et al. 2010). The postulated beginning of Intra-oceanic  
173 obduction was around Toarcian to Bajocian time (180–170 Ma), based  
174 on the ages of amphibolites found in the “metamorphic sole” of  
175 subduction-zone mélanges (Roddick et al. 1979; Spray and Roddick  
176 1980; Spray et al. 1984). The platform subsided during the Middle  
177 Jurassic, verified by ever deepening carbonate facies (Scherreiks 2000),  
178 and then became emergent during Callovian time, verified by bauxite  
179 deposits (Fig. 4a) (Scherreiks et al. 2016). The age of this Callovian  
180 upheaval has been verified with Bathonian foraminifera in the limestones  
181 below, and Oxfordian foraminifera above the bauxite crusts (Table 1a 5  
182 and 6) (ibid.). The “Callovian event” has been attributed to plate tectonic  
183 stress that affected the entire Mediterranean region (Meléndez et al.  
184 2007). An Oxfordian transgression re-established shallow marine  
185 environments which generated a Tethys-wide reef facies that extended  
186 from the Alps to Asia and in the Hellenides is characterised by the

187

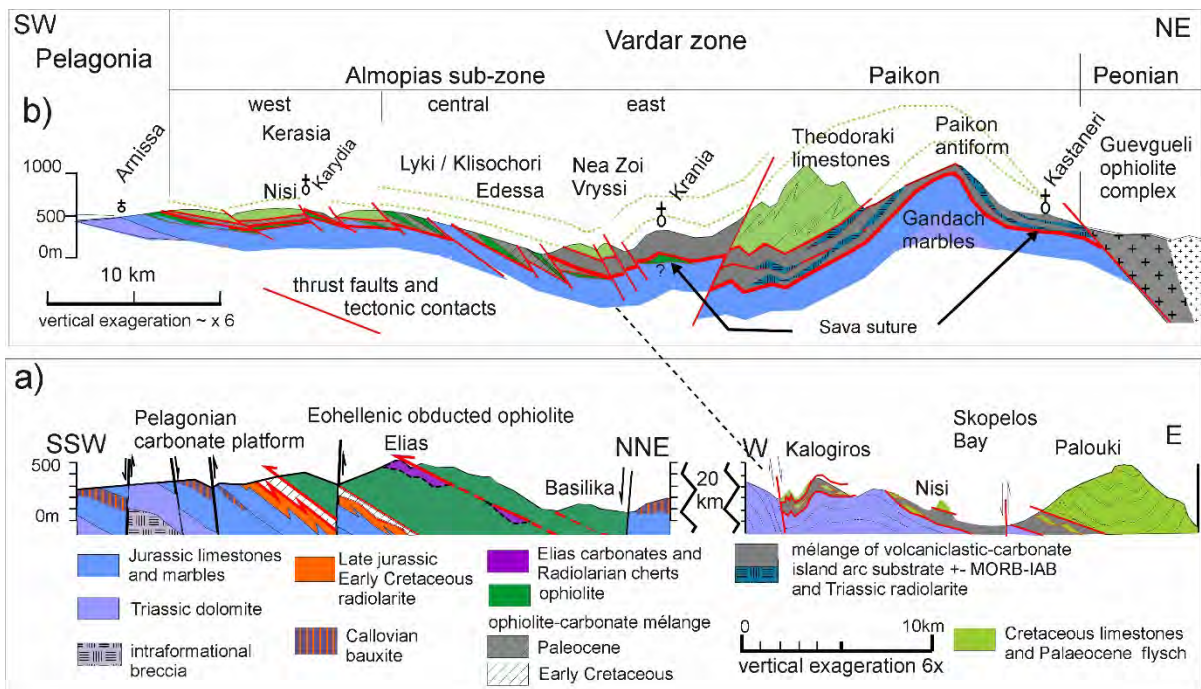


Fig. 4 (see figure captions)

demosponge, *Cladocropsis mirabilis* Felix (Flügel 1974; Scherreiks 2000) (Table 1a 7 and 8). Rapid platform subsidence and drowning below the CCD occurred during Tithonian-Berriasian time, verified by radiolarian cherts (Baumgartner and Bernoulli, 1976). The final ophiolite emplacement is estimated to have occurred in Valanginian time, in Evvoia, after flysch-like sedimentation had been shut off by the obduction (Scherreiks 2000; Scherreiks et al. 2010; Scherreiks et al. 2014). The obduction was followed by a period of ophiolite erosion (post-Eohellenic unconformity: Scherreiks 2000) and a subsequent gradual, widespread, transgression of marine conglomerate in Evvoia and across the Pelagonian zone during Early Cretaceous time (Fazzuoli et al. 2008; Photiades et al. 2018; Scherreiks 2000) (Table 1a 9).

### ***Palaeogeography of the Vardar ocean discerned from seismic tomographic images of the mantle below the Hellenides***

Seismic tomographic images of the Alpine-Himalayan realm (BSE models, Bijwaard et al. 1998) depict mantle-perturbations of subducted slabs of Neotethys oceanic lithosphere (Bijwaard and Spakman 2000; Hafkenscheid 2004; van der Meer et al. 2018).

Van Hinsbergen and others (2005) recognised two separate and distinct perturbations in tomographic images as probable Neotethys slabs. For our investigations, we have enlarged the tomographic images of the areas below the Hellenides and have discerned that there are two slabs (Fig. 3a-c). To check this out, we looked further eastwards to the Arabian Sea (Fig. 3d) and have corroborated that two slabs of oceanic



216 lithosphere have subducted there also. Figure 3d, in detail, is highly  
217 interpretive, however, two distinct parallel perturbations are apparent.  
218 We have interpreted the perturbations beneath Hellenides as sunken  
219 Vardar ocean lithosphere and are of the opinion that the images verify  
220 two episodes of subduction (Scherreiks and BouDagher-Fadel 2020a)  
221 (Fig. 3c) (see Discussion and conclusions).

222

## 223 **The study areas**

224

### 225 ***Evvoia and Northern Sporades***

#### 226 ***Ophiolites and Platforms***

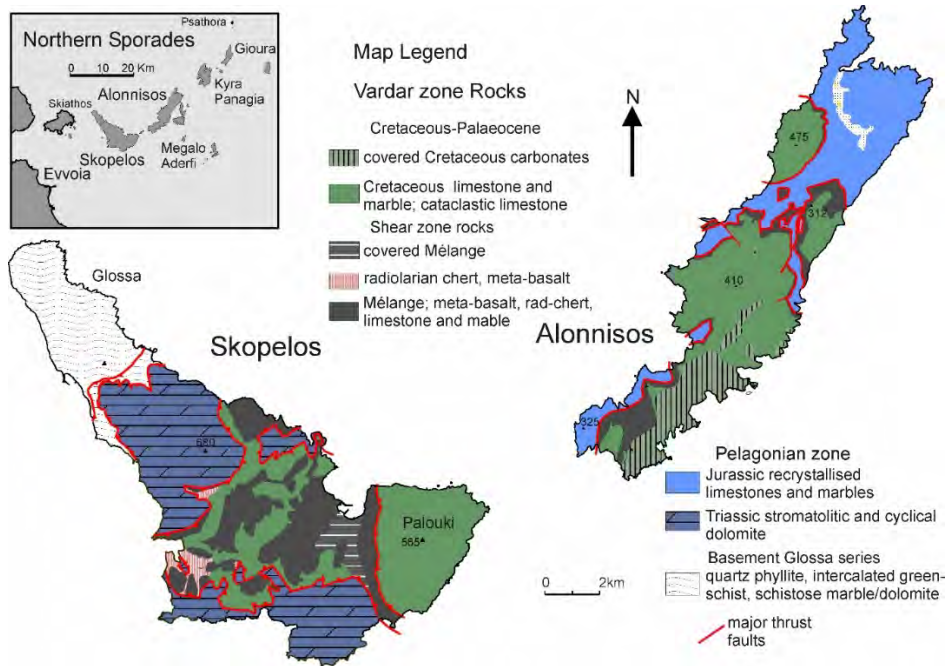
227 Examples of obducted ophiolite s. str. occur in the study areas of  
228 northern Evvoia (Fig. 4a) (Scherreiks 2000; Scherreiks et al. 2014) and  
229 are found throughout the Korab-Pelagonian zone (Fig. 1). They lie,  
230 tectonically emplaced, together with mélangé on top of Upper Jurassic  
231 and Lower Cretaceous carbonate platform rocks (Jacobshagen et al.  
232 1976; Jacobshagen 1986). The ophiolites are erosional remnants that  
233 have been postulated to be parts of a single obducted ophiolite sheet  
234 that was emplaced during the Late Jurassic to Early Cretaceous, an age  
235 which classifies it as “Eohellenic” after Jacobshagen et al. (1976). The  
236 onetime ophiolite sheet is considered to have had a width of at least  
237 200km - when judged from the width of the ophiolite outcrops on  
238 geologic maps (Gawlick et al. 2008; Schmid et al., 2020) (Fig. 1).

239

240 The Northern Sporades are devoid of serpentinite. The ophiolite sheet,  
241 known to have been obducted over Pelagonia, had been eroded from  
242 large areas of Pelagonia during later Lower Cretaceous time (see  
243 above). On the Sporades, erosion was extreme; the ophiolite and large  
244 parts of the carbonate platform are missing (Fig. 5). The eroded surface  
245 of Jurassic and Triassic platform carbonates is covered by a sheet of  
246 mélangé composed of meta-basalt and radiolarian chert which is  
247 chaotically mixed with carbonate breccia and mylonitic phyllonites  
248 (Scherreiks and BouDagher-Fadel 2020a) (Fig. 4a and Fig. 5). Slices of  
249 Cretaceous and Paleocene platform carbonates of reefal origins are  
250 tectonically incorporated in the mélangé (Table 1a 10-10.3). The  
251 Cretaceous carbonate platform successions of Alonnisos and Skopelos  
252 overlie the mélangé. In corroboration with Kelepertsis (1974) we suggest  
253 that the Cretaceous and Paleocene carbonates of the northern  
254 Sporades are of Vardar zone origin, which will be expanded upon in the  
255 Discussion and Conclusions. The Cretaceous carbonate platform and its  
256 mélangé substrate, we suggest, correlate with a similar succession in  
257 the Almopias sub-zone (Fig. 4a-b).

258

259  
260  
261



262  
263  
264

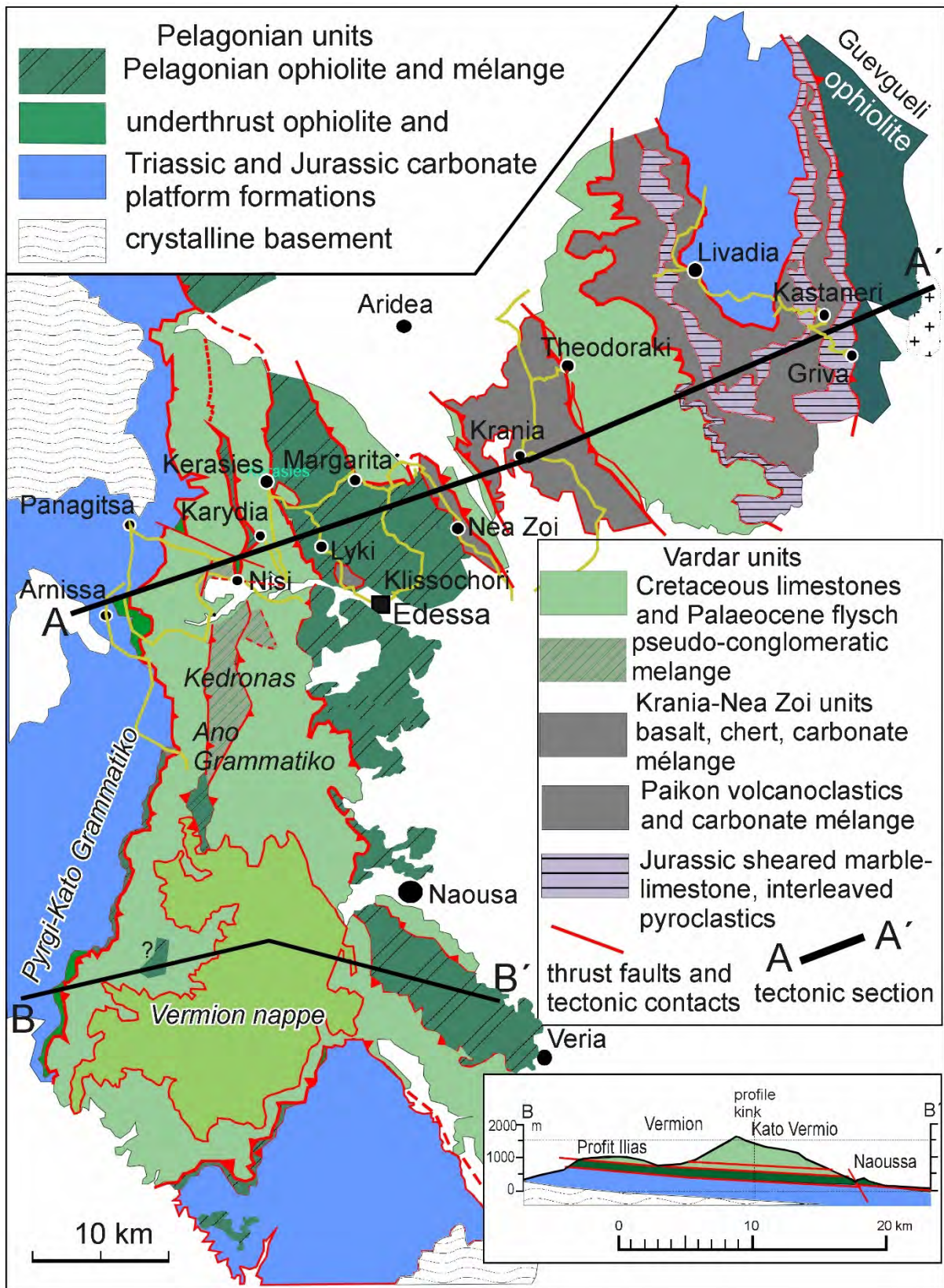
Fig. 5 (see figure captions)

265  
266

### **The Vardar zone West Almopias and its tectonic contact with Pelagonia**

267  
268  
269  
270  
271  
272  
273  
274  
275  
276  
277  
278  
279  
280  
281  
282  
283  
284  
285

Sheared Eohellenic ophiolite occurs on top of Pelagonian carbonates in contact with disrupted Cretaceous limestones (Table 1b 1 and 2), along the western border of the Vardar zone, for example near Panagitsa and Arnissa Fig. 6) (Mercier and Vergely 1988) and southwards near Pyrgi-Kato Grammatiko and west of the Vermion mountains (Georgiadis et al. 2016) (Fig. 6). West verging imbricated thrust faults characterise this western boundary of the Vardar zone, from the Dinarides through the Hellenides (in Jacobshagen (1986) from Mercier (1973), Mercier and Vergely (1979)). The base of the imbricates is Eohellenic ophiolite and the Triassic-Jurassic carbonate platform of the Pelagonian zone which is covered by disrupted ophiolite followed by schistose pyroclastic units interleaved with slices of radiolarian cherts, volcanoclastic and chloritic marble layers. This tectonic transition between Pelagonia and the western edge of the Vardar zone is shown by Sharp and Robertson (2006) in the Arnissa area (Fig. 6): a ~500-metre-thick succession of imbricated ophiolite mélangé. This succession is topped off by limestone debris with Rudists and Planktonic foraminifera, *Globo truncana* (Mercier and Vergely 1988) (Table 1b 3) (Plate 1). In agreement with these



286

287

288 Fig. 6 (see figure captions)

289

290 observations, we underscore that the contact between the Vardar and  
 291 Pelagonian zone is a thrust-fault-zone (see Discussion).

292 Although Cretaceous carbonates have been supposed to *transgressively*  
293 overlie laterite and serpentinite (Mercier and Vergely 1988; Sharp and  
294 Robertson 2006; Photiades et al. 2018), we are of the opinion that the  
295 inferred transgressional conglomerates are cataclasites (Plate 2a-b) and  
296 that orthoconglomerates (Friedman 2003) that could substantiate a  
297 marine transgression have not been verified (see Discussion and  
298 conclusions). Furthermore, the Cretaceous limestones of the Vardar  
299 zone are in tectonic contact with the subjacent allochthonous substrate  
300 even where post-Eohellenic laterite is found along the contacts. The  
301 circumstances here are similar to the Northern Sporades where a  
302 *sedimentary* contact of the Cretaceous Carbonates with their original  
303 substrate is nowhere to be found (Scherreiks and BouDagher-Fadel  
304 2020a).

305

### 306 ***Tectonic windows in west Almopias***

307 Serpentinite and ophiolite-carbonate mélange crop out through the  
308 Cretaceous limestone cover in tectonic windows along a narrow,  
309 elongated zone of north-south striking faults, extending from Kerassia-  
310 Karydia-Kedronas (Mercier and Vergely 1972; 1988) to Ano Grammatiko  
311 (Sacciani et al. 2008; Georgiadis et al. 2016) (Fig. 6). Extensive  
312 exposures consist of “conglomeratic” rocks (Mercier and Vergely 1988),  
313 which in our opinion are cataclasites (see Plate 2 and Discussion). The  
314 “conglomeratic” rocks contain Triassic and Jurassic carbonates as well  
315 as limestones ranging in age from Cenomanian to Turonian (Table 1b2)  
316 and overlie Pelagonian serpentinite (ibid.). Near Nisi and Karydia (Fig. 6)  
317 these cataclasites (Plate 2a-b) occur below Campanian limestone (Table  
318 1b 4) (Plate 1). At its base, this succession contains olistolith marbles of  
319 Triassic-Jurassic age and overlie white micaceous Triassic marbles in  
320 suggested *transgressional* contact (ibid). We dispute a transgressional  
321 origin of the Kedronas-Nisi “conglomerate” (see discussion on pseudo-  
322 conglomerates). The tectonic windows exposing underthrust Pelagonian  
323 ophiolite rocks can be followed in west Almopias from the north near  
324 Karydia to the Vermion area (Georgiadis et al., 2016) (Fig. 6, see section  
325 B-B’).

326

### 327 ***Pelagonian ophiolite exposures of central Almopias***

328 An extensive imbricated belt of ophiolite mélange some 50 kilometres  
329 long and 5-10 kilometres wide can be traced from the Lyki-Klissochori  
330 area (Mercier and Vergely 1984; 1988) to the Naousa and Veria areas  
331 (Fig. 6) (Saccani et al. 2008; 2015; Georgiadis et al. 2016). The mélange  
332 is interleaved with slices of marble and Jurassic carbonates, which we  
333 agree, are of Korab-Pelagonia origin (Bortolotti et al 2013; Georgiadis et  
334 al. 2016) (Table 1b 6 and 7-7.2). The carbonates contain an Oxfordian-



335 Kimmeridgian reefal fauna, including *Cladocoropsis* sp. of Late Jurassic  
336 age (Mercier and Vergely 1984). As pointed out above, this is a typical  
337 Kimmeridgian-Tithonian reef facies of the Pelagonian zone (Scherreiks  
338 2000) (Table 1a 7-8) that had been overthrust by Eohellenic ophiolite  
339 during the Early Cretaceous. In the Vardar zone, the Pelagonian  
340 ophiolites are locally interleaved with sericitized basalt schist (Lyki) (see  
341 Geochemistry) and are in underthrust position beneath “conglomeratic”,  
342 ophiolitic mélange and upper Cretaceous carbonates (east of Margarita,  
343 Fig. 6) (Table 1b 7).

344 In accord with the afore cited researchers and the described geology, we  
345 support the opinion that the ophiolites and Upper Jurassic carbonates  
346 found in the west and central Vardar sub-zones are tectonically inherited  
347 from the underthrust Pelagonian plate (Fig. 4b).

348

### 349 ***Eastern Almopias and Paikon units***

350 A noteworthy difference between the eastern and western units of the  
351 Vardar zone is that the eastern Almopias and the Paikon units appear to  
352 be devoid of serpentinite which we corroborate from Tranos et al., 2007.  
353 Serpentinite, however, probably exists at depth (Fig. 4b), because  
354 further north in an area known as Ano Garefi serpentinitized peridotite is  
355 exposed below basalt (saccani et al. 2015). The mélanges of the Nea  
356 zoi-Vryssi-Meglenitsa and Krania units (Fig. 4b and Fig. 6) are  
357 composed of dolerite, pillow basalt and tuff and contain upper Jurassic-  
358 lower Cretaceous radiolarite (Mercier and Vergely 1984), with a relict  
359 Cretaceous cover (Table 1c 1.-1.2). Slices of Triassic lavas and  
360 radiolarites (Stais et al. 1990) (Table 1c 3 and 4) and upper Cretaceous  
361 arenites are also incorporated into the foliated matrix of the mélange of  
362 the Krania-Vryssi units (Saccani et al. 2015). The “*ophiolite related*”  
363 mafic units, “*ophiolite nappe*” and “*Meglenitsa Ophiolite*”, reported in  
364 Sharp and Robertson 2006 (from Sharp and Robertson 1994 and Sharp  
365 & Robertson 1998), in our opinion are not ophiolites s. str. but consist of  
366 ocean floor or arc basaltic rocks (see Geochemistry).

367

### 368 ***The Paikon antiform, a Pelagonian window: Katrivanos et al. 2013***

369 The Theodoraki limestone is the youngest formation of the Paikon  
370 antiform (Katrivanos et al. 2013). This limestone is part of the  
371 Cretaceous carbonate platform that covers the entire Vardar zone, and  
372 is composed of a wide range of neritic to reefal facies (Table 1b and  
373 Table 1c Theodoraki unit). The platform is in tectonic contact with a pile-  
374 up of SW dipping slices of Theodoraki limestones and slices of volcano-  
375 sedimentary rocks including radiolarites, tuffites and lava, and Triassic-  
376 Jurassic Marble and schist of Pelagonian origin (Mercier and Vergely  
377 2002). Katrivanos and others (2013) corroborate that the tectono-



378 stratigraphic sequence is composed of volcano-clastic rocks together  
379 with limestones of Middle to Late Jurassic age, based on micro and  
380 macro-faunas including *Cladocoropsis mirabilis* (Griva-Kastaneri  
381 formation Fig. 4b, Fig. 6) (Table 1c Griva-Khromni units). The volcano-  
382 sedimentary slices are on top of Triassic-Jurassic Gandatch marbles  
383 and schists (Fig. 6). All the volcanic material of this series is *strongly*  
384 *mylonitized in discrete, narrow shear zones* related to mylonitic foliation  
385 (Katrivanos et al. 2013). The carbonate rocks are mylonitized, near the  
386 contacts with tectonically overlying volcano-sedimentary slices e.g., at  
387 Kastaneri (ibid). Our investigations corroborate the above observations,  
388 which lead us to interpret the volcano-sedimentary formations in the  
389 substrate of the Theodoraki limestone as a composite allochthonous  
390 mélange complex in which slices of volcanic and sedimentary rock-units  
391 can be individually distinguished.

392 In contrast to the above, the Paikon unit has been depicted (Sharp and  
393 Robertson 1994) to consist of a contiguous sedimentary, stratigraphic,  
394 succession extending from the Triassic to Cretaceous time only  
395 interrupted by two unconformities, an Oxfordian and a Cenomanian.

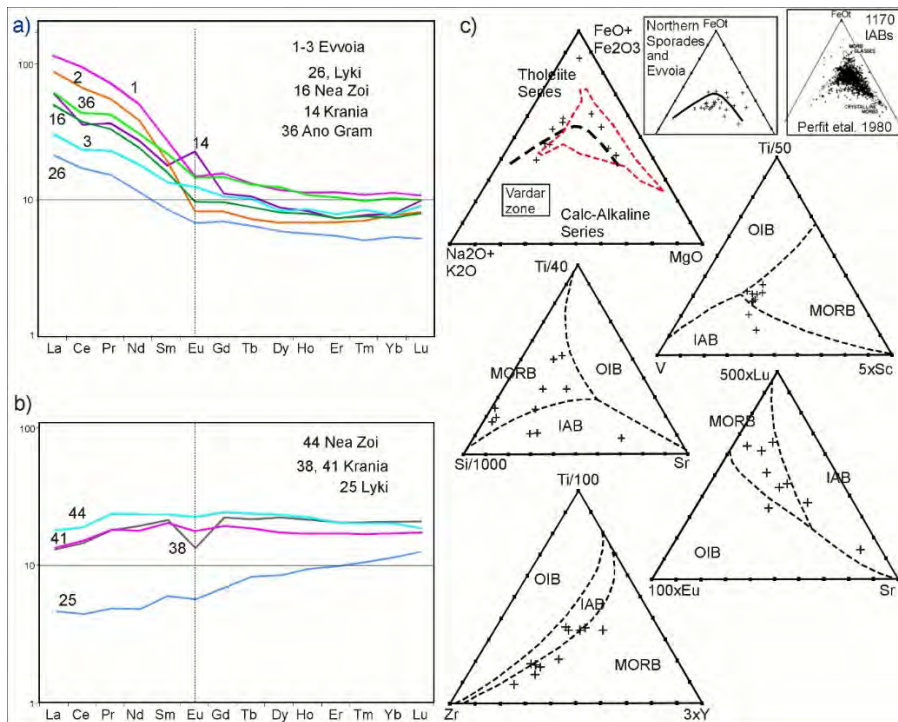
396  
397 We share the opinion that the Paikon is an antiform and a Pelagonian  
398 tectonic window (Katrivanos et al. 2013), and that the Paikon unit of the  
399 Vardar zone was most probably part of a volcanic island arc complex  
400 (Mercier et al. 1975; Mercier et al. 2002; BeBien et al. 1994; Brown &  
401 Robertson 2004; Mercier and Vergely 2002; Saccani et al. 2015, Schmid  
402 et al. 2020). Our mutually envisioned island arc scenario evolved as the  
403 eastern Vardar ocean subducted north-eastwards towards the margin of  
404 the European continent, which initiated supra-subduction arc volcanism  
405 (Mercier and Vergely 2002; Brown and Robertson, 2004; Saccani et al.,  
406 2015). This was accompanied by back-arc spreading (Hafkinscheid,  
407 2004; Schmid et al. 2020), represented by the Guevgueli ophiolite  
408 complex (Fig. 4b) (Anders et al. 2005; Saccanni et al. 2008b; Bortolotti  
409 et al. 2013; Michail et al. 2016).

410

### 411 **Geochemistry**

412 Meta-basalts from the Vardar zone and from northern Evvoia have been  
413 analysed for their major, minor and trace element contents, and some  
414 previous analyses are shown from the Northern Sporades (Scherreiks  
415 and BouDagher-Fadel 2020a). The analytical results are in Tables 2a  
416 and 2b. Rare-Earth (REE) plots and ternary discrimination diagrams  
417 (Fig. 7) have been drafted for the purpose of ascertaining basalt origins  
418 (after Pearce and Cann 1973; Perfit et al. 1980; Vermeesch P, 2006).

419



420

421 Fig. 7 (see figure captions)

422

423 Two serpentinized peridotites associated with basalts and radiolarian  
 424 cherts from Pelagonian ophiolites of Evvoia were previously analysed  
 425 (Scherreiks and BouDagher-Fadel 2020a) (Table 2b).

426 The meta-basalts of the Vardar zone and the Northern Sporades occur  
 427 in mélanges and they are sheared and sericitized and strongly  
 428 weathered, which may have caused contaminations with adjacent rocks,  
 429 making unambiguous differentiation between MORB and island IAB  
 430 additionally more problematic than it intrinsically is anyway (as Perfit and  
 431 others, 1980, point out). None of the analyses (Table 2a) have abnormal  
 432 Cr or Ni contents which excludes serpentinite contamination (compare  
 433 Cr and Ni Table 2b samples 2-3).

434 The REE plots are typical for basalts (Pearce and Cann 1973; Kay and  
 435 Hubbard 1978; Perfit et al. 1980; Hooper and Hawkesworth 1993) (Fig,  
 436 6a and 6b). They depict light REE (LREE), enhanced patterns,  
 437 associated with IABs, and flat LREE-depleted patterns associated with  
 438 MORB origins. An almost identical array of REE plots have been  
 439 ascertained for the Northern Sporades where the present authors had  
 440 drawn the conclusion that MORBs and IABs had been tectonically mixed  
 441 in the mélanges of an extensive thrust-fault zone (Fig. 7) (Scherreiks  
 442 and BouDagher-Fadel 2020a). As in the Northern Sporades, the REE-  
 443 plots drafted for the Vardar zone indicate the presence of both IAB and  
 444 MORB (Fig. 7a-b). Discrimination diagrams (Fig. 7c) also indicate the

445 ambiguous situation that MORBs for samples in one diagram  
446 correspond to IABs in another.  
447 Following Perfit and others (1980) we have additionally checked out that  
448 according to Perfit (ibid) there are distinguishing differences in  
449 potassium, titanium, and total iron wt.% concentrations in IABs and  
450 MORBs: MORBs having <0.25 K<sub>2</sub>O, IAB having >0.25 K<sub>2</sub>O; IAB having  
451 <1.2 TiO<sub>2</sub>, and >6-15 total Fe. The results of this query, using data from  
452 tables 2a and 2b, it appears that most of our samples are IABs but there  
453 are numerous ambiguities which, presumably, are caused by tectonic  
454 mélangé mixing.  
455 The analyses of the basalts from the Eohellenic ophiolite of Evvoia and  
456 those of the Elias complex are incorporated in the REE and AFM  
457 diagrams (Fig. 7a and c) (Table 2b) and they indicate MORB and IAB  
458 affinities.

459

## 460 **Discussion and conclusions**

461

### 462 ***The composite tectono-stratigraphy of eastern Pelagonia and the*** 463 ***Vardar zone in context with the afore related geology***

464 Pelagonia consists of a Palaeozoic-Middle Triassic basement covered  
465 by a carbonate platform over which a 200 km-wide ophiolite sheet of  
466 west Vardar ocean lithosphere, had been obducted (Fig. 8a, b, c). The  
467 1700 km-wide eastern Vardar ocean subducted beneath the Vardar  
468 zone (vz) during Late Jurassic through Cretaceous time (Fig. 8c). Figure  
469 8a - b suggests that Pelagonia together with obducted Eohellenic  
470 ophiolite collided with the Vardar zone and underthrusts the Cretaceous-  
471 carbonate-platform and its volcano-sedimentary substrate (Fig. 8 b). As  
472 Pelagonia continued to advance it underthrust the Guevgueli complex  
473 and crashed with Serbo-Macedonia (Fig. 8b, c).

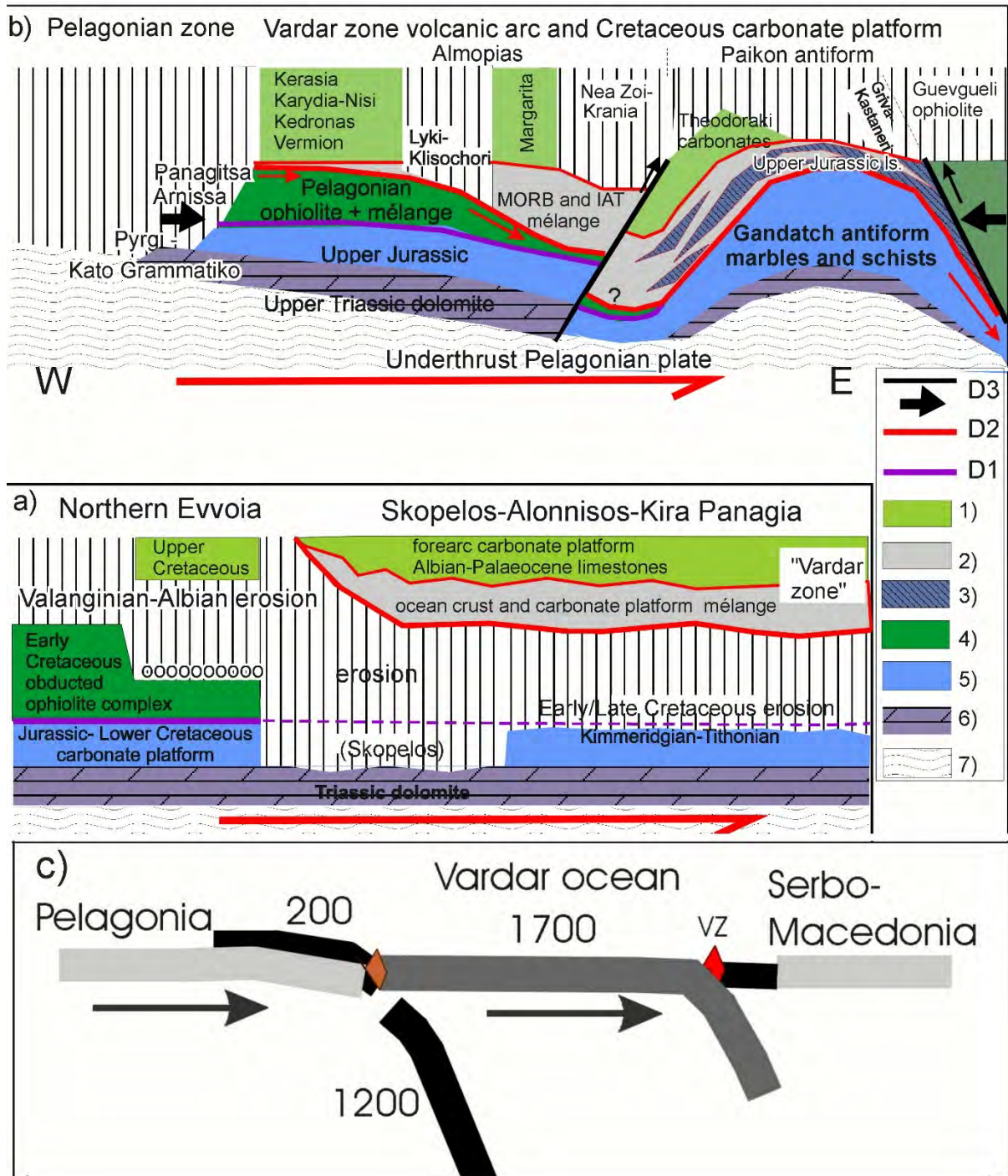
474

### 475 ***Major deformations***

476 Three major episodes of tectonic deformation, D1-D3, affected the  
477 Pelagonian and Vardar zones; each dominated by a major time-  
478 transgressive thrust fault complex (Fig. 8a-b). D1 and D2 occur in both  
479 study areas; D3 is evident in the Vardar zone but has not been verified  
480 in the Northern Sporades (Fig. 8a-b). (Our D1-D3 indices do not  
481 correspond with those of previous researchers (Mercier and Vergely  
482 2002; Kiliyas et al. 2010; Katrivanos et al. 2013).

483

484



485  
486  
487  
488  
489  
490  
491  
492  
493

Fig. 8 (see figure captions)

Deformation D1, is Eohellenic (Fig. 8a), involving the westward obduction of the Eohellenic (west Vardar ocean) ophiolite onto eastern Pelagonia (Fig. 8c). Post-D1 erosion, especially prominent in Skopelos, is suggested to have been caused by widespread Pelagonian uplift as the sinking Vardar (1200km) slab broke off in post-Valanginian time (Fig.8c).

494 Deformation D2: Pelagonia, the trailing edge of the eastward subducting  
495 Vardar plate, crashed with and underthrust the Vardar arc, causing  
496 shearing, mylonitisation, and imbrication between the overriding  
497 Cretaceous carbonate platform including its volcano-sedimentary  
498 substrate. Greenschist and HP/LT metamorphism described by  
499 Katrivanous et al. 2013 can be attributed to D2.

500 Deformation D3 corresponds to the compression effected by the crash of  
501 the Pelagonian plate with Serbo-Macedonia, which caused folding in the  
502 Vardar and Pelagonian zones whereby the Paikon antiform is the most  
503 prominent (Fig. 8b). An analogical antiform has not been observed in the  
504 Northern Sporades but could be sought in the central Aegean sea (Fig.  
505 8a). Shear-stress caused by the crash produced the youngest thrust  
506 faults in the flanks of the Paikon antiform (D3 in Fig. 8b) and most  
507 probably rejuvenated older faults, including numerous subordinate  
508 imbrication thrusts (Fig. 4b), described in Mercier and Vergely (2002),  
509 Kiliyas et al. (2010) and Katrivanos et al. (2013).

510

### 511 ***Pseudo conglomeratic mélange of Kedronas, Nisi and Karydia***

512 The breccio-conglomeratic, cataclastic rock complex that contains  
513 abundant rounded clasts occurs incorporated in an extensive fault zone  
514 mélange in the west Almopias unit between Karydia and Ano  
515 Grammatiko (Plate 2a-b) (Fig. 6 pseudo conglomeratic mélange). In the  
516 Nisi-Karydia area the cataclasites are in tectonic contact with  
517 Campanian limestones on top (Plate 1) (Table 1b 4.1) and Pelagonian  
518 ophiolite at the base. We regard the cataclasites as matrix supported  
519 parabreccias composed of poorly sorted >2mm, rounded to angular  
520 clasts (Plate 2a-b). The clasts either consist predominantly of marbles,  
521 elongated pieces of sericitic calc-schists and dark micritic limestones  
522 (Plate 2b) or are chaotic mixtures of carbonate and ophiolite clasts  
523 (Plate 2a). Viewed under the microscope, the matrix is a chaotic breccia  
524 of calcite and carbonate grains that are not bound by interstitial pore  
525 cement (Bathurst 1976) but by insular patches of aggrading neomorphic  
526 sparry calcites that had grown amid the much smaller angular granules  
527 of the matrix (Plate 2c, d, e). Crushed neomorphic calcite occurs in the  
528 matrix inherited from earlier stages of shearing. The neomorphic calcite,  
529 unlike cement, exhibits irregular boundaries and palimpsest, relic-matrix  
530 texture (Plate 2 d-e). The neomorphic calcites exhibit residual stress,  
531 indicated by crossing twins, stopping twins, twin thickening, and  
532 bending, which appears in low temperature stress regimes below 200  
533 °C. (Burkhard 1993; Chen et al, 2011). Neomorphism had most likely



534 taken place in a dry sub-metamorphic environment (Folk 1965 in  
535 Bathurst 1976).  
536 It is suggested that the larger components underwent rounding and  
537 grain-reduction by granulation from the decimetre to centimetre scale to  
538 microscopic micron scale, which is not unusual in tectonic breccias in  
539 which the fragments may be worn down and rounded by tectonic  
540 grinding (Norton 1917; Higgins 1971; Woodcock and Mort 2008).  
541 We dispute that this rock complex had a transgressional origin (Mercier  
542 and Vergely 1988; and Mercier 1966 in Sharp and Robertson 2006)  
543 because it does not display the most important characteristics that  
544 marine conglomerates should have: clast-clast support and diagenetic  
545 cement (Bathurst 1976; Friedman 2006). On the contrary the clasts are  
546 matrix supported and the grains have not been diagenetically cemented.  
547 In our opinion the “parabreccio-conglomerate” formed as Pelagonia  
548 underthrust the Vardar zone during Paleocene time (D2 above).

549

### 550 **The collision of two Cretaceous carbonate platforms**

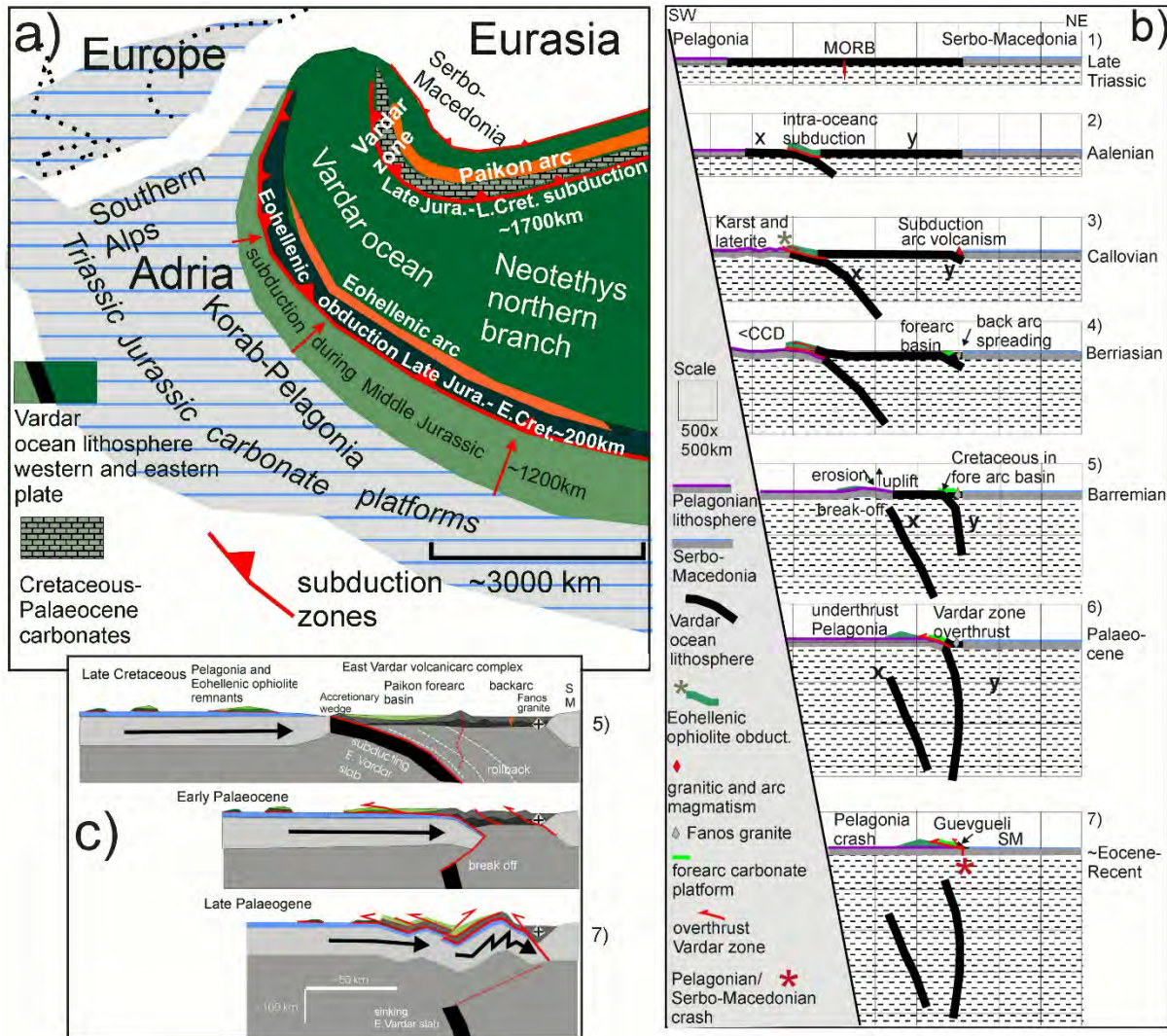
551 It should be taken into consideration that some remnants of the well  
552 documented Cretaceous Pelagonian carbonate platform (Fig. 8a), may  
553 have been subducted (“piggy-backed”) beneath the Cretaceous  
554 carbonate platform of west Almopias, at the latest during Paleocene  
555 time, and thus inherited Pelagonian-orthoconglomerates possibly could  
556 occur in the mélanges beneath the Vardar zone (e.g., Vermion:  
557 Photiades et al. 2018).

558

### 559 **New Palaeogeography**

560 From evidence presented above and from seismic tomography it is  
561 postulated that the Vardar ocean subducted along two subduction zones  
562 (Fig. 9a). The western intra-oceanic subduction zone evolved about  
563 Toarcian to Aalenian time, based on radiometric ages of amphibolites in  
564 sub-ophiolite mélanges, and continued to subduct through the Middle  
565 Jurassic verified by late Middle Jurassic radiolarians in the sub-ophiolite  
566 mélange in Evvoia (Danelian and Robertson 2001; Gingins and  
567 Schauner 2005; Scherreiks et al. 2014) (Table 1a 11.2 and 12). A supra-  
568 subduction volcanic arc evolved during the Middle Jurassic, documented  
569 by the Elias complex of northern Evvoia (Fig. 4a) which presumably was  
570 part of a more extensive supra-subduction “Eohellenic arc” (Fig. 9a)  
571 (ibid.). The beginning of the Eohellenic obduction, is suggested to have  
572 begun during Bathonian time together with the Callovian upheaval  
573 (Meléndez et al. 2007) and the eastward subduction of the eastern

574 Vardar ocean (Fig. 9b3). The Vardar, supra-subduction, volcanic island  
 575 arc and the spreading Guevgueli back arc ophiolite complex evolved  
 576 during (Middle?) Late Jurassic and Cretaceous time. We envisage a  
 577 Paikon forearc basin, rimmed by an accretionary wedge like that shown  
 578 in Saccani et al. (2008b) in which the basin floor was initially covered by  
 579



580  
 581 Fig. 9 (see figure captions)

582  
 583 (volcanoclastic) basalt without carbonates during the lower Middle  
 584 Jurassic. To our knowledge, a Jurassic carbonate platform did not  
 585 evolve in the Vardar zone. We suggest that Jurassic-Early Cretaceous  
 586 volcanoclastic deposits accumulated on the flanks of the Vardar volcanic  
 587 arc and became the substrate of carbonate accumulation beginning in  
 588 Aptian time. Investigations of the Guevgueli back arc basin have not  
 589 disclosed relicts of a carbonate platform (Saccani et al. 2008b).

590  
 591 **The Cretaceous forearc carbonate platform of the Vardar zone**

592 The Cretaceous Vardar-zone carbonate platform is envisaged to have  
593 evolved over the late Jurassic-early Cretaceous volcanoclastic substrate  
594 of the forearc basin (Fig. 9a) (Fig. 12 in Saccanni et al. 2008b).

595 The earliest recorded Cretaceous limestones in the Vardar zone are of  
596 Aptian age (Table 1b4.2, Table 1c6.1). The bio facies indicate a reefal to  
597 inner neritic environment having had depths of between 10 and 50m  
598 (BouDagher-Fadel 2018a). These limestones are in the west Almopias  
599 sub-zone (Fig. 4b) and may have been deposited near or on the  
600 accretionary wedge of the forearc basin (Saccanni et al. 2008b). The  
601 verified bio facies indicate that patch reef and neritic environments  
602 existed side by side through Cenomanian, Santonian, Campanian, and  
603 Maastrichtian time (Table 1b West Almopias) (Plate 1). The deeper  
604 neritic platform facies occur eastwards in the central and east Almopias  
605 sub zones, ranging in age from the Cenomanian to Maastrichtian (Table  
606 1b-c Central and East Almopias). The bio stratigraphic succession in the  
607 Theodoraki limestone formation begins with Cenomanian/Turonian reef  
608 facies that may represent a fringing reef along the outer slopes of the  
609 arc. Inner neritic facies deepen upwards, from the Campanian to  
610 Maastrichtian times (Table 1c 5 Theodoraki unit). Late Maastrichtian  
611 flysch signals the demise of the Cretaceous carbonate platform of the  
612 Vardar zone.

613 From the afore said, a tentative picture of the platform-architecture can  
614 be discerned: it was a subsiding environment in which about 500 m of  
615 carbonates accumulated ("carbonate factory" Schlager 2000) during  
616 about 60Ma between Aptian and Maastrichtian time (Mercier and  
617 Vergely 1984, 1988). Reefs evolved during Early Cretaceous along an  
618 outer western accretionary wedge and inner eastern high where fringing  
619 reefs on the outer slopes of the Paikon volcanic arc interdigitated outer  
620 neritic carbonate facies in the central basin.

621

### 622 **Seismic tomographic images of the mantle below the Hellenides**

623 We have interpreted the perturbations beneath Hellenides as sunken  
624 Vardar ocean lithosphere which indicate two episodes of subduction  
625 (Scherreiks and BouDagher-Fadel 2020a) (Fig. 3c).

626 The vertical section (Fig. 3c) shows that the leading edges of each slab  
627 has sunk to a depth approaching 2000 kilometres. Presently, the trailing  
628 edge of the western slab (x in Fig. 3c) is about 900 kilometres below the  
629 Earth's surface and the trailing edge of slab (y) is about 400 kilometres  
630 below the surface. These are the depths to which the slabs have sunk  
631 since their breakoffs. In estimating the width of a slab, however, one

632 must consider that a subsiding lithospheric plate certainly undergoes  
633 compression and deformation which can make width-estimates  
634 inaccurate (Fig 3e). The seismic tomographic images are, nevertheless,  
635 presently the best possible way to estimate the onetime width of the  
636 subducted oceanic lithosphere which we estimate to have been about  
637 3000 kilometres (determined by adding together the lengths of the slabs  
638  $(x + y) \sim 1200 + \sim 1700$  and adding, to that sum, the width of the  
639 obducted Eohellenic ophiolite sheet which has been assumed to be  
640 about  $\sim 200$  kilometres (Fig. 8c)). However, 3100km is the composite  
641 width, not necessarily the surface width that the Vardar ocean had at  
642 any one time. We do not know when the ocean ridge stopped spreading:  
643 subduction and ocean spreading at the ocean ridge could have taken  
644 place simultaneously.

645 The western slab (x) is supposed to have broken off and began sinking  
646 after the Eohellenic ophiolite had been emplaced during Valanginian  
647 time. The eastern Almopias slab (y) is supposed to have broken off after  
648 Pelagonia crashed and underthrust the Vardar-zone carbonate platform  
649 and volcanic arc complex.

650

### 651 ***Seismic tomographic model***

652 Our model (Fig. 9) postulates that the Vardar ocean was about 3000km  
653 wide and bordered on Adria in the west. This means that both the  
654 microplate Adria and the vaguely attached African plate, were situated  
655 3000km further southwest during Early Jurassic time as the Atlantic  
656 Ocean and the Alpine Tethys began spreading (e.g., Schmid et al. 2008;  
657 Scherreiks et al. 2010). This implies that Pelagonia, the eastern edge of  
658 Adria, moved about 3000km northeast towards the European continent  
659 (Fig. 9b) while the Atlantic spread.

660 The  $\sim 3000$ km wide Vardar ocean is supposed to have  
661 subducted/obducted, between ( $\sim$ Sinemurian) Aalenian time (175 Ma)  
662 and Paleocene time ( $\sim 65$  Ma), roughly a time span of  $175 - 65 = 110$ Ma.  
663 Subduction rates of the oceanic slabs are estimated to range from about  
664 3 cm/year (= 30km/1Ma) in the upper mantle to about 1 cm/year in the  
665 lower mantle (Norton 1999). Simple calculations show that at a rate of  
666 30km/1Ma, a 3300km wide ocean would subduct in 110 Ma; and a  
667 3000km wide ocean could subduct in 110Ma at a rate of  $\sim 2.7$ cm/a.  
668 In our example, we also consider that the trailing edge of Slab X sank  
669 900 km since breaking off after Valanginian time, and the trailing edge of  
670 slab Y sank about 400 km since its breakoff in the  $\sim$ Paleocene.

671 Sinking rates are lower in the mantle below 300–500 km, and in the  
672 lower mantle slab subsidence eventually approaches zero (Lallemand  
673 and Funiciello 2009; Ichikawa et al. 2016). We have previously  
674 estimated (Scherreiks and BouDagher-Fadel 2020a. 2020b) that in using  
675 an average subsidence rate of 0.68 cm/year, one arrives at a  
676 Hauterivian break-off date for slab X (900km/6.8km/Ma ~132 Ma), and  
677 Late Paleocene as the break-off time of slab Y (400 km/6.8 km/Ma ~59  
678 Ma), which we believe corresponds to the known facts and is well in the  
679 range of plausibility.

680

### 681 **Summary**

682 The demise of the once over 3000-kilometre-wide Vardar ocean has  
683 been reconstructed from field investigations of its remnants in its  
684 onetime peripheries, and from seismic tomographic images of its  
685 remnants in the Mantle below the Central Hellenides. On its  
686 southwestern side the Vardar ocean bordered on the Pelagonian-  
687 Adriatic plate which was covered by a vast carbonate platform  
688 (BouDagher-Fadel and Bosence 2007) that evolved from a peritidal  
689 realm during Norian-Sinemurian- to a drowned platform during  
690 Tithonian-Berriasian-time. In the northeast the Vardar ocean bordered  
691 on Serbo-Macedonia of the European plate, where, during the Late  
692 Jurassic a supra-subduction volcanic island arc and back-arc complex  
693 emerged. A forearc reef and a shallow marine carbonate platform  
694 accumulated on top of a Jurassic-Early Cretaceous volcano-clastic  
695 substrate from about Aptian through Maastrichtian time.  
696 The closure of the Vardar ocean occurred in temporally overlapping  
697 episodes: one episode of ophiolite obduction and two episodes of intra-  
698 oceanic subduction.

- 699 1. During Middle Jurassic time a 1200-kilometre slab of west Vardar  
700 lithosphere subducted eastwards beneath the “Eohellenic”, arc,  
701 while a 200-kilometre-wide slab obducted westwards onto  
702 Pelagonia between Callovian and Valanginian time.
- 703 2. A 1700-kilometre-wide slab of east Vardar lithosphere subducted  
704 eastwards beneath the Vardar-zone arc-complex during Late  
705 Jurassic through Cretaceous time and subsequently Pelagonia  
706 underthrust the Cretaceous carbonate platform during the  
707 Paleocene.

708 In the greater framework of plate tectonics, the subduction of the Vardar  
709 ocean occurred simultaneously with the spreading of the Atlantic Ocean



710 and the opening of the Alpine Tethys, while the Hellenides moved about  
711 3000 kilometres toward the northeast.

712 In the light of the present contribution, future research concerning the  
713 evolution of the Cretaceous carbonate platform of the Vardar zone could  
714 advance our knowledge of the facies distributions and architecture of the  
715 Paikon fore arc basin. Another point of interest is the seismic  
716 tomography and the demise of the Guevgueli back arc since Paleocene  
717 time.

## 718 **Acknowledgements**

719 *University College London:*

720 We are grateful to the Office of the Vice-Provost (Research, Innovation,  
721 and Global Engagement), especially Prof. David Price, for helping and  
722 facilitating our research.

723 *The Bayerische Staatssammlung für Palaeontologie und Geologie and*  
724 *the Department of Earth and Environmental Sciences, Ludwig*  
725 *Maximilian University, Munich, through Prof. Anke Friedrich and Dr.*  
726 *Winfried Werner, are acknowledged for supporting this research which*  
727 *turned out to become an over 20-year project for which we gratefully*  
728 *thank Prof. Peter Baumgartner (Lausanne), Prof. Dan Bosence*  
729 *(London), Dr. Georgia Fermeli (Athens) and Prof. Guillermo Meléndez*  
730 *(Saragossa) for their most valued previous field and co-author*  
731 *participations. We thank ACTIVATION LABORATORIES LTD., Ancaster,*  
732 *Ontario, for carrying out the geochemical analyses. Special thanks are*  
733 *given Michael Born, Bonn, Germany for the preparation of thin sections.*  
734 *We are indebted to Prof Robert Hall, Royal Holloway, University of*  
735 *London, for carefully and thoroughly reviewing our paper.*

## 736 **References**

- 737 Anders, B., Reischmann, T., Poller, U., Kostopoulos, D. (2005) Age and origin of  
738 granitic rocks of the eastern Vardar Zone, Greece: new constraints on the  
739 evolution of the Internal Hellenides. *J. Geol. Soc. London*, 162: 857-870.
- 740 Bathurst, R. G. C. (1976) Carbonate sediments and their Diagenesis. *Dev in*  
741 *Sedimentol* 12, Elsevier, 658pp
- 742 Baumgartner P. O., Bernoulli D. (1976) Stratigraphy and radiolarian fauna in a Late  
743 Jurassic–Early Cretaceous section near Achladi (Evvoia, Eastern Greece).  
744 *Ecl Geol Helv* 69:601–626
- 745 Baumgartner, P.O., Bartolini, A., Carter, E.S., Conti, M., Cortese, G., Danelian, T.,  
746 De Wever, P., Dumitrica, P., Dumitrica-Jud, R., Gorican, S., Guex, J., Hull,  
747 D.M., Kito, N., Marcucci, M., Matsuoka, A., Murchey, B., O'Dogherty, L.,  
748 Savary, J., Vishnevskaya, V., Widz, D. and Yao, A., (1995) Middle Jurassic to

749 early cretaceous radiolarian biochronology of Tethys based on unitary  
750 associations. In: Baumgartner, P.O. et al., eds., Middle Jurassic to lower  
751 cretaceous Radiolaria of Tethys: occurrences, systematics, biochronology,  
752 Mém. Géol., (Lausanne), 23, 1013-1048.

753 BeBien, J., Voet, P. B., Mercier, J. (1994): Geodynamic significance of the Paicon  
754 massif in the Hellenides: Contribution of the volcanic rock studies. *Bulletins of*  
755 *the Geological Society of Greece*, 30/1: 63-67.

756 Bernoulli, D., Manatschal, G., Desmurs, L., Müntener, O. (2003) Where did Gustav  
757 Steinmann see the trinity? Back to the roots of an Alpine ophiolite concept. in  
758 Dilek, Y., and Newcomb, S., eds., *Ophiolite concept and the evolution of*  
759 *geological thought: Boulder, Colorado, Geological Society of America Special*  
760 *Paper 373*, p. 93–110.

761 Bijwaard, H., Spakman, W. (2000) Non-linear global P-wave tomography by iterated  
762 linearized inversion. *Geophys. J. Int.* 141, 71-82

763 Bijwaard, H.W., Spakman, W., Engdahl, E.R. (1998) Closing the gap between  
764 regional and global travel time tomography. *J. Geophys. Res.*, 103, 30,055–  
765 30,078

766 Bortolotti, V., Chiari, M., Marroni, M., Pandolfi, L., Principi, G., Saccani, E. (2013)  
767 Geodynamic evolution of ophiolites from Albania and Greece (Dinaric-Hellenic  
768 belt): one, two, or more oceanic basins? *Int J Earth Sci* 102:783-811

769 Bosellini, A. (1984) Progradation geometries of carbonate platforms: examples from  
770 the Triassic of the Dolomites, northern Italy. *Sedimentology*, 31, 1-24

771 Bosence, D. (2005) A genetic classification of carbonate platforms based on their  
772 basinal and tectonic settings in the Cenozoic. *Sediment Geol* 175:49–72

773 Bosence, D., Procter, E., Aurell, M., Atef Bel, K., BouDagher-Fadel, M., Casaglia, F.,  
774 Cirilli, S., Mehdie, M., Nieto, L., Rey, J., Scherreiks, R., Soussi, M. and  
775 Waltham, D., (2009) A dominant tectonic signal in high-frequency, peritidal  
776 carbonate cycles? A regional analysis of Liassic platforms from western  
777 Tethys, *J. Sed. Res.*, 79(5-6), 389-415.

778 BouDagher-Fadel, M.K., Bosence, D.W.J. Early Jurassic benthic foraminiferal  
779 diversification and biozones in shallow-marine carbonates of western Tethys.  
780 *Senckenbergiana lethaea* 87, 1–39 (2007).

781 BouDagher-Fadel, M. K. (2008) The Mesozoic larger benthic foraminifera: the  
782 Jurassic. In: Boudagher-Fadel, M.K., ed., *Evolution and geological*  
783 *significance of larger benthic foraminifera*, Wignall PB (series ed) *Dev*  
784 *Palaeontol Strat* 21, Elsevier, Amsterdam.

785 BouDagher-Fadel, M.K., (2015) *Biostratigraphic and Geological Significance of*  
786 *Planktonic Foraminifera (Updated 2nd Edition)*. London: UCL Press.  
787 doi:10.14324/111.9781910634257.

788 BouDagher-Fadel, M.K. (2018a) *Evolution and Geological Significance of Larger*  
789 *Benthic Foraminifera*, Second ed. UCLPress, London. 704 pp.

790 BouDagher-Fadel, M. K. (2018b) Revised diagnostic first and last occurrences of  
791 Mesozoic and Cenozoic planktonic foraminifera. UCL Office of the Vice-  
792 Provost Research, Professional Papers Series, 1-5.

- 793 BouDagher-Fadel, M., & Price, G. D. (2019) Global evolution and paleogeographic  
794 distribution of mid-Cretaceous orbitolinids. UCL OPEN - ENVIRONMENT.  
795 doi:10.14324/111.444/ucloe.000001
- 796 Brown, S., Robertson, A. (1994) New structural evidence from the Mesozoic-early  
797 Tertiary Paicon unit, Northern Greece. *Bull Geol Soc Greece*, 30/1: 159-170
- 798 Brown, S.A.M., Robertson, A.H.F. (2004) Evidence for Neotethys rooted within the  
799 Vardar suture zone from the Voras Massif, northernmost Greece.  
800 *Tectonophysics* 381, 143e173.
- 801 Burkhard, M. (1993) Deformation mechanisms and fabric Calcite twins, their  
802 geometry, appearance and significance as stress-strain markers and  
803 indicators of tectonic regime: a review. *Jour of Structural Geol*, 15, 3–5, 351-  
804 368
- 805 Chen, K., Kunz, M., Tamura, N. et al. (2011) Deformation twinning and residual  
806 stress in calcite studied with synchrotron polychromatic X-ray microdiffraction.  
807 *Phys Chem Minerals* 38, 491–500
- 808 Chiari, M., Marcucci, M. (2003) Triassic and Jurassic radiolarian assemblages from  
809 the siliceous sediments associated with pillow lavas in the Argolis Peninsula  
810 (Greece). *Abstr Tenth Meeting International Association Radiolarian*  
811 *Palaeontologists*, Lausanne: 40
- 812 Chiari, M., Bortolotti, V., Marcucci, M., Photiades, A., Principi, G., Sacconi, E. (2012)  
813 Radiolarian biostratigraphy and geochemistry of the Koziakas massif  
814 ophiolites (Greece). *Bull. Soc. géol. France*, 183, no 4, 289-309.
- 815 Danelian, T., Robertson, A.H.F. (2001) Neotethyan evolution of eastern Greece  
816 Pagondas Mélange, Evia island inferred from radiolarian biostratigraphy and  
817 the geochemistry of associated extrusive rocks. *Geol Mag* 138:345–363
- 818 Fazzuoli, M., Menna, F., Nirta, G., Bortolotti, V., Carras, N., Principi, G. (2008) The  
819 Cretaceous transgression in the Dinaric-Hellenic orogen. *Soc. Geol. It.*, 6,  
820 Nuova Serie
- 821 Flügel, E. (1974) Fazies-Interpretation der Cladocoropsis-Kalke (Malm) auf  
822 Karaburun, W-Anatolien. *Arch Lagerstforsch (Ostalpen) Sonderbd* 2, Leoben,  
823 79-94
- 824 Flügel, E. (1983) Mikrofazies der Pantokrator-Kalke (Lias) von Korfu, Griechenland.  
825 *Facies* 8: 263-300
- 826 Friedman, G.M. (2003) Classification of sediments and sedimentary rocks. In Gerard  
827 V. Middleton, ed., pp. 127-135, *Encyclopedia of Sediments & Sedimentary*  
828 *Rocks*, Encyclopedia of Earth Science Series. Kluwer Academic Publishers,  
829 Boston, Massachusetts. 821 pp. ISBN 978-1-4020-0872-6
- 830 Froitzheim, N., Jahn-Awe, S., Frei, D., Wainwright, A.N., Maas, R., Georgiev, N.,  
831 Nagel, J.T., Pleuger, J. (2014) Age and composition of meta-ophiolite from the  
832 Rhodope Middle Allochthon (Satovcha, Bulgaria): a test for the maximum-  
833 allochthony hypothesis of the Hellenides. *Tectonics* 33(8):1477–1500
- 834 Fruth, I., Scherreiks, R. (1982) Hauptdolomit (Norian) – stratigraphy, paleogeography  
835 and diagenesis. *Sedimentary Geol*, 32: 195-231
- 836 Gallhofer, D., von Quadt, A., Schmid, S.M., Guillong, M., Peytcheva, I., Seghedi, I.  
837 (2017) Magmatic and tectonic history of Jurassic ophiolites and associated

838 granitoids from the South Apuseni Mountains (Romania). *Swiss J. Geosci.*  
839 110, 699-719

840 Gawlick, H.-J., Frisch, W., Hoxha, L., Dumitrica, P., Krystyn, L., Lein, R., Missoni, S.,  
841 Schlagintweit, F. (2008) Mirdita zone ophiolites and associated sediments in  
842 Albania reveal Neotethys ocean origin. *Int J Earth Sci (Geol Rundsch)*  
843 97:865–881

844 Georgiadis, G.A., Tranos, M.D., Kiliyas, A.A., Mountrakis, D.M. (2016) The  
845 emplacement of the Vermion nappe in the area of Kato Seli (Mt. Vermion  
846 Central Macedonia, Greece. *Bull. Geol. Soc. Greece*, vol. L, 24-33  
847 *Proceed. 14th Intern. Congr. Thessaloniki*

848 Gingins, Y., Schauner, O. (2005) *Etude géochimique et paléontologique des*  
849 *séries Maliaques d'Othrys et du complexe d'Elias, Eubée du Nord, Grèce.*  
850 *Diss Université de Lausanne, Manuscript February 2005, 1–93pp*

851 Hafkenscheid, E. (2004) *Subduction of the Tethys Oceans reconstructed from plate*  
852 *kinematics and mantle tomography. Thesis, Faculty of Geosciences Utrecht*  
853 *University, The Netherlands. ISBN: 90-5744- 101-200.*

854 Higgins, M.W. (1971) *Cataclastic Rocks. Geol Surv Professional Paper 687, U S*  
855 *Government Print Office, Washington Library of Congress Catalog No. 71-*  
856 *611932; 1971.*

857 Hooper, P.R., Hawkesworth, C.J. (1993) *Chemical characteristics of island arc*  
858 *basalts. J Petrol.* 1993; 34:1203–46

859 Hsü, K.J. (1974) *Melanges and their distinction from olistostromes. In: Dott RH,*  
860 *Shaver RH (eds) Modern and ancient geosynclinal sedimentation. Soc Econ*  
861 *Paleontol Mineral Spec Publ 19: 321-333*

862 Ichikawa, H., Yamamoto, S., Kawai, K., Kameyama, M. (2016) *Estimate of*  
863 *subduction rate of island arcs to the deep mantle. J Geophys Res Solid Earth.*  
864 2016; 121:5447–60.

865 Jacobshagen, V., Risch, H., Roeder, D. (1976) *Die Eohellenische Phase. Definition*  
866 *und Interpretation. Zeitschr Deutsche Geol Gesell.* 1976;127: 133–45.

867 Jacobshagen, V., (1986) *Geologie von Griechenland. In: Beiträge Zur Regionalen*  
868 *Geologie der Erde Band 19. Gebrüder Bornträger, Berlin, 363 pp*

869 Katrivanos, E., Kiliyas, A., Mountrakis, D. (2013) *Kinematics of deformation and*  
870 *structural evolution of the Paikon Massif (Central Macedonia, Greece): A*  
871 *Pelagonian tectonic window? N. Jb. Geol. Paläont. Abh.* 269/2, 149–171

872 Kay, R.W., Hubbard, N.J. (1978) *Trace elements in ocean ridge basalts. Earth*  
873 *Planet Sci Lett.* 38:95–116.

874 Kelepertsis, A. (1974) *Geological structure of Alonnisos and Peristera islands. Z dt*  
875 *geol Ges;125: 225–36.*

876 Kendall, G.St.C., Schlager, W. (1981) *Carbonates and relative changes in sea level.*  
877 *In: Cita MB, Ryan WBF (eds) Carbonate platforms of the passive-type*  
878 *continental margins, present and past. Mar Geol* 44: 181–212

879 Kiliyas, A., Frisch, W., Avgerinas, A., Dunkl, I., Falalakis, G., Gawlick, H.-J. (2010)  
880 *Alpine architecture and kinematics of deformation of the northern Pelagonian*  
881 *nappe pile in the Hellenides. Austrian Journal of Earth Sciences Volume*  
882 *103/1 4-28*

883 Kockel, F. (1979) in: Die Vardar- (Axios-) Zone. Jacobshagen, V., Geologie von  
884 Griechenland, Gebrüder Borntraeger Berlin-Stuttgart, pp. 150-168.

885 Lallemand, S., Funicello, F., (2009) editors: Royden, Leigh H. (et al.) Subduction  
886 with Variations in Slab Buoyancy: Models and Application to the Banda and  
887 Apennine Systems. Subduction zone geodynamics; 35. Springer-Verlag,  
888 Berlin, Heidelberg, 272pp. ISBN 978-3-540-87974-9

889 Matarangas, D. (1992) Geological investigations of Skopelos island (North  
890 Sporades, Greece). D 188 (Diss. Freie Universität Berlin) Berichte des  
891 Forschungszentrums Jülich, 2684,157.

892 Meléndez, G., Ramajo, J., Bello, J., D'Arpa, C., Di Stefano, P., Fermeli, G.,  
893 Karakitsios, V., Mallarino, G., Mindszenty, A., Scherreiks, R., Zarcone, G.  
894 (2007) Palaeogeographic and palaeontologic event across the Tethys, in the  
895 Submediterranean and Mediterranean platforms at the Callovian-Oxfordian  
896 transition. XXIII Jornadas de la Sociedad Espanola de Paleontologia  
897 (Caravaca de la Cruz, Libro de Resúmenes:139–140

898 Meneghini, F., Marroni, M., Moorw, J.C., Pandolfi, L., Rowe, C.D. (2009) The  
899 processes of underthrusting and underplating in the geologic record: structural  
900 diversity between the Franciscan Complex (California), the Kodiak Complex  
901 (Alaska) and the Internal Ligurian Units (Italy). *Geol. J.* 44: 126–152

902 Mercier, J. (1968) Etude géologique des zones Internes des Hellenides en  
903 Macedoine centrale. Contribution à l'étude du métamorphisme et de l'  
904 évolution magmatique des zones internes des Hellenides. – *Annales*  
905 *Géologique des Pays Héliéniques* 20, 1-739.

906 Mercier, J., Vergely, P., Geological Map of Greece 1.50.000 - Sheet Arnissa (1988)  
907 Institute of Geology and Mineral Exploration, Athens

908 Mercier, J., Vergely, P., Geological Map of Greece 1.50.000 - Sheet Edhessa (1984)  
909 Institute of Geology and Mineral Exploration, Athens

910 Mercier, J. L., Vergely, P. (1972) Le mélanges ophiolitiques de Macédoine (Grèce) :  
911 décrochements d'âge anté-Crétacé supérieur. *Z. Deutsch, geol. Ges.*,  
912 Hannover, 123, 469-489.

913 Mercier, J.L., Vergely, P., 2002. The Paikon massif revisited, comments on the Late  
914 Cretaceous e paleogene geodynamics of the Axios-Vardar Zone. How many  
915 Jurassic ophiolitic basins? (Hellenides, Macedonia, Greece). *Bull. Geol. Soc.*  
916 *Greece* 34/6, 2099-2112. doi: org/10.12681/bgsg.16852.

917 Michail, M., Pipera, K., Koroneos, A., Kiliyas, A., Ntaflos, T. (2016) New perspectives  
918 on the origin and emplacement of the Late Jurassic Fanos granite, associated  
919 with an intra-oceanic subduction within the Neotethyan Axios-Vardar Ocean.  
920 Published online: 26 March 2016 Springer-Verlag Berlin Heidelberg 2016

921 Norton, W.H. (1917) A Classification of Breccias. *The Journal of Geology*, Vol. 25,  
922 No. 2, 160-194

923 Norton, I. O. (1999) Global plate reconstruction model report. Texas (USA):  
924 Exxon Mobil Exploration

925 Pearce, J.A., Cann, J.R. (1973) Tectonic setting of basic volcanic rocks determined  
926 using trace element analyses. *Earth Planet Sci Lett.* 1973; 19:290–300.



927 Perfit, M.R., Gust, D.A., Bence, A.E., Arculus, R.J., Taylor, S.R., (1980) Chemical  
928 characteristics of island-arc basalts: Implications for mantle sources.  
929 Chemical Geology Volume 30, Issue 3, 227-256

930 Photiades, A., Carras, N., Bortolotti, V., Fazzuoli, M. (2018) The late Early  
931 Cretaceous transgression on the laterites in Vourinos and Vermion massifs  
932 (western Macedonia, Greece). Bulletin of the Geological Society of Greece  
933 40(1):182

934 Robertson, A. (2004) Development of concepts concerning the genesis and  
935 emplacement of Tethyan ophiolites in the Eastern Mediterranean and Oman  
936 regions. Earth Sci Rev 66:331–387

937 Robertson, A.H.F., Trivić, B., Đerić, N., Bucur, I. (2013) Tectonic development of the  
938 Vardar ocean and its margins: Evidence from the Republic of Macedonia and  
939 Greek Macedonia. Tectonophysics 595–596, 25–54

940 Roddick, J.C., Cameron, W.A., Smith, A.G. (1979) Permo-Triassic and Jurassic  
941  $^{40}\text{Ar}/^{39}\text{Ar}$  ages from Greek ophiolites and associated rocks. Nature 279:788–  
942 790

943 Saccanni, E., Photiades, A., Santato, A., Zeda, O. (2008a) New evidence for supra-  
944 subduction zone ophiolites in the Vardar zone of northern Greece:  
945 Implications for the tectonic-magmatic evolution of the Vardar ocean basin  
946 *Ofioliti*, 2008, 33 (1), 65-85

947 Saccanni, E., Bortolotti, V., Marroni, M., Pandolfi, L., Photiades, A., Principi, G.  
948 (2008b) The Jurassic association of backarc basin ophiolites and calc-alkaline  
949 volcanics in the Guevgueli complex (Northern Greece): Implications for the  
950 evolution of the Vardar Zone. *Ofioliti* 33 (2), 209-227

951 Saccanni, E., Chiari, M., Bortolotti, V., Photiades, A., Principi, G. (2015) Geochemistry  
952 of volcanic and subvolcanic rocks and biostratigraphy on radiolarian cherts  
953 from the Almopias ophiolites and Paikon unit (Western Vardar, Greece).  
954 *Ofioliti* 40,1-25. <https://doi.org/10.4454/ofioliti.v40i1.432>.

955 Scherreiks, R. (1998) The evolution of a passive margin in response to plate  
956 tectonics, eustacy, and an advancing ophiolite nappe (Jurassic, NE-Evvoia,  
957 Greece). *Terra Nostra* 98: 72-73

958 Scherreiks, R. (2000) Platform margin and oceanic sedimentation in a divergent and  
959 convergent plate setting (Jurassic, Pelagonian Zone, NE Evvoia, Greece). *Int*  
960 *J Earth Sci* 89:90–107

961 Scherreiks, R., Bosence, D., BouDagher-Fadel, M., Meléndez, G., Baumgartner,  
962 P.O. (2010) Evolution of the Pelagonian carbonate platform complex and the  
963 adjacent oceanic realm in response to plate tectonic forcing (Late Triassic and  
964 Jurassic), Evvoia, Greece. *Int J Earth Sci* 99:1317–1334

965 Scherreiks, R., Meléndez, G., Fermeli, G., Baumgartner, P.O., BouDagher-Fadel, M.,  
966 Bosence, D. (2011) A time-transgressive ophiolite-platform collision (late  
967 Middle Jurassic to Early Cretaceous, Pelagonian zone, Evvoia, Greece).  
968 *Fragile Earth: GV-GSA meeting, LMU München Paper 19-9*

969 Scherreiks, R., Meléndez, G., BouDagher-Fadel, M., Fermeli, G., Bosence, D. (2014)  
970 Stratigraphy and tectonics of a time-transgressive ophiolite obduction onto the  
971 eastern margin of the Pelagonian platform from Late Bathonian until

972 Valanginian time, exemplified in northern Evvoia, Greece, *Int. J. Earth Sci.*,  
973 103, 2191-2216.

974 Scherreiks, R., Meléndez, G., BouDagher-Fadel, M., Fermeli, G., Bosence, D.  
975 (2016) The Callovian unconformity and the ophiolite obduction onto the  
976 Pelagonian carbonate platform of the Internal Hellenides. *Bulletin of the  
977 Geological Society of Greece*, vol. L; Proceedings of the 14th Intern.  
978 Congress, Thessaloniki, May 2016

979 Scherreiks, R., BouDagher-Fadel, M. (2020a) Tectono-stratigraphic correlations  
980 between Northern Evvoia, Skopelos and Alonnisos, and the postulated  
981 collision of the Pelagonian carbonate platform with the Paikon forearc basin  
982 (Pelagonian-Vardar zones, Internal Hellenides, Greece). *UCL Open*

983 Scherreiks, R., BouDagher-Fadel, M. (2020b) The closure of the Neotethys in two  
984 episodes: as a result of Late Jurassic to Early Cretaceous obduction and  
985 Early Paleocene collision, based on surface geology and tomographic models  
986 (Internal Hellenides, Greece) Conference: Tectonics, geodynamics, and  
987 paleogeography of the Alpine-Himalayan orogen from the Earth's mantle to its  
988 surface at: Utrecht virtual oral presentation 26.08.2020 Session 3.3 ID 112

989 Schmid, S.M., Bernoulli, D., Fügenschuh, B., Matenco, L., Schefer, S., Schuster, R.,  
990 et al. (2008) The Alpine-Carpathian-Dinaridic orogenic system: correlation and  
991 evolution of tectonic units. *Swiss J Geosci.* 101:139–83.

992 Schmid, S.M., Fügenschuh, B., Kounov, A., Matenco, L., Nievergelt, P., Oberhänsli,  
993 R., et al. (2020) Tectonic units of the Alpine collision zone between Eastern  
994 Alps and western Turkey. *Gondwana Res.* 78:308–374.

995 Sengör, A.M.C., Natal'in, B.A. (1996) Paleotectonics of Asia: fragments of a  
996 synthesis, in: *The Tectonic Evolution of Asia*, eds Yin A, Harrison T.M., 486–  
997 640, Cambridge University Press.

998 Sharp, I.R., Robertson, A.H.F. (1994) Late Jurassic–Lower Cretaceous oceanic crust  
999 and sediments of the eastern Almopias Zone, NW Macedonia (Greece);  
1000 implications for the evolution of the eastern “Internal” Hellenides. *Bull Geol  
1001 Soc Greece* 30:47–61

1002 Sharp, I. R. & Robertson, A. H. F. (1998) Late Jurassic-Lower Cretaceous oceanic  
1003 crust and sediments of the Eastern Almopias Zone, NW Macedonia (Greece);  
1004 implications for the evolution of the Eastern 'Internal' Hellenides. *Bulletin of  
1005 the Geological Society of Greece*, 30(1), 47-61.

1006 Sharp, I.R., Robertson, A.H.F. (2006) Tectonic-sedimentary evolution of the western  
1007 margin of the Mesozoic Vardar Ocean: evidence from the Pelagonian and  
1008 Almopias zones, northern Greece. In: *Tectonic development of the Eastern  
1009 Mediterranean Region*. Robertson AHF, Mountrakis D (Eds.), *Geol. Soc.  
1010 London Spec. Publ.*, 260: 373-412.

1011 Simantov, J., Economou, C., Bertrand, J. (1991) Metamorphic rocks associated with  
1012 the Central Euboea ophiolite (southern Greece): some new occurrences. In:  
1013 Malpus J, Moores EM, Panayiotou A, Xenophontos C (eds) *Ophiolites,  
1014 oceanic crustal analogies*. *Proc Symp Troodos 1987*, Geol Surv Dept  
1015 Nicosia/Cyprus, pp 285-293

1016 Schlager, W., (2000) Sedimentation rates and growth potential of tropical, cool-water  
1017 and mud-mound carbonate systems. In *Insalaco, E., Skelton, P. W., and*

- 1018 Palmer, T. J. (eds.), Carbonate Platform Systems: Components and  
 1019 Interactions. London: The Geological Society, pp. 217–227.
- 1020 Spakman, W., van der Lee, S., van der Hilst, R.D. (1993) Travel-time tomography of  
 1021 the European^Mediterranean mantle down to 1400 km, Phys. Earth planet.  
 1022 Inter., 79, 3-74.
- 1023 Spray, J.G., Roddick, J.C (1980) Petrology and Ar geochemistry of some Hellenic  
 1024 subophiolite metamorphic rocks. Contrib Mineral Petrol 72:43–55
- 1025 Spray, J.G., Bebieu, J., Rex, D.C., Roddick, J.C. (1984) Age constraints on the  
 1026 igneous and metamorphic evolution of the Hellenic±Dinaric ophiolites. Geol  
 1027 Soc Lond Spec Publ 17 : 619±627
- 1028 Stais, A., Ferriere, J., Caridroit, M., De Wever, P., Clement, B., Bertrand, J. (1990)  
 1029 Donnees nouvelles sur l'histoire ante-obduction (Trias- Jurassique) du  
 1030 domaine d'Almopias (Macedoine, Grece). Comptes Rendus de l'Academie de  
 1031 Sciences, Serie II, 310, 1275-1480.
- 1032 Stampfli, G.M., Borel, G.D. (2004) The TRANSMED transects in space and time:  
 1033 Constraints on the paleotectonic evolution of the Mediterranean domain, in  
 1034 The TRANSMED Atlas: the Mediterranean Region from Crust to Mantle. eds  
 1035 Cavazza, W., Roure, F., Spakman, W., Stampfli, G.M., Ziegler, P.A., Springer
- 1036 Tranos, M. D., Plougarlis, A. P., Mountrakis, D. M. (2007) A new consideration  
 1037 about the Almopias-Paikon boundary based on the geological mapping in the  
 1038 area of Nerostoma-Lakka (Central Macedonia, Greece)  
 1039 Proceedings of the 11th International Congress, Athens, May,
- 1040 Ustaszewski, K., Kounov, A., Schmid, S.M., Schaltegger, U., Krenn, E., Frank, W.,  
 1041 Fügenschuh, B. (2010) Evolution of the Adria-Europe plate boundary in the  
 1042 northern Dinarides: from continent–continent collision to back-arc extension.  
 1043 Tectonics 29:1-34
- 1044 van der Meer, D.G., van Hinsbergen, D.J.J., Spakman, W. (2018) Atlas of the  
 1045 underworld: Slab remnants in the mantle, their sinking history, and a new  
 1046 outlook on lower mantle viscosity. Tectonophysics 723, 309–448
- 1047 van Hinsbergen, D.J.J., Hafkenscheid, E., Spakman, W., Meulenkamp, J.E., Wortel,  
 1048 M.J.R. (2005) Nappe stacking resulting from subduction of oceanic and  
 1049 continental lithosphere below Greece. Geology 33, 325–328.
- 1050 van Hinsbergen, D.J.J., Torsvik, T.H., Schmid, S.M., Matenco, L.C., Maffione, M.,  
 1051 Gürer, D., Vissers, R.L.M. (2019) Companion paper. Orogenic architecture of  
 1052 the Mediterranean region and kinematic reconstruction of its tectonic evolution  
 1053 since the Triassic. Gondwana Res.
- 1054 Vermeesch, P. (2006) Tectonic discrimination diagrams revisited. Geochem  
 1055 Geophys Geosyst Am Geophys Union 7(6):1–55
- 1056 Woodcock, N.H., Mort, K. (2008). Classification of fault breccias and related fault  
 1057 rocks. Geological Magazine, 145(3), 435-440.
- 1058 Zimmerman, J., Ross, J.V. (1976) Structural evolution of the Vardar root zone,  
 1059 northern Greece. Bull Geol Soc Am 87: 1547-1550

1060

## 1061 **Figure Captions**

1062

1063 **Fig. 1: Neotethys lithosphere** oceanic lithosphere in the Dinarides through the Hellenides and  
 1064 Taurides, represent remnants of the northern branch of the Neotethys (altered after Ustaszewski et al.

1065 2010). Our study areas are in Evvoia and the Northern Sporades, and in the “Vardar zone” of Greek  
1066 Macedonia. Fieldwork was carried out in the Vardar zone and Northern Evvoia in September and  
1067 October 2020 and Evvoia and the Northern Sporades in previous years.  
1068

1069 **Fig. 2 Palaeogeography and evolution of the Vardar ocean** (a) altered after Stampfli and Borel,  
1070 2004; (b) altered after Schmid et. al. 2008; Gallhofer et al 2017 and Van Hinsbergen et al. 2019, in  
1071 Schmid et al, 2020)

1072 a) The Vardar domain of the Northern Tethys ocean evolved out of the Maliac and Paleotethys in  
1073 Permo-Triassic time.

1074 b) The Vardar ocean was situated between continental Adria (including Korab-Pelagonia) and Serbo-  
1075 Macedonian Europe. The paleogeography implies that early Middle Jurassic intra-oceanic subduction  
1076 led to the obduction of the Eohellenic ophiolite onto eastern Pelagonia and, subsequently, that Vardar  
1077 ocean lithosphere subducted beneath the Paikon island arc and led to the collision of eastern  
1078 Pelagonia with the island arc. See text.  
1079

1080 **Fig. 3 Seismic tomographic images below the Central Hellenides**

1081 a) Map sketch of the Hellenides shows the position of the NE-SW vertical section through the mantle  
1082 below the Central Hellenides c).

1083 b) Seismic tomographic images (BSE models, ascertained from Hafkenscheid 2004) of horizontal  
1084 sections through the mantle at 6 different depths. They depict contours of seismic velocity anomalies  
1085 (see Hafkenscheid 2004 for the theoretical background).

1086 c) The vertical section through the BSE models. The sketch schematically depicts perturbation  
1087 “clouds” containing the lithospheric “slabs” (see e)). Slab X has sunk about 900km, slab Y has sunk  
1088 about 400km.

1089 d) Vertical sections depicting the mantle eastwards of the Hellenides show that there are two sinking  
1090 lithospheric slabs. Positions of sections are shown in BSE Model 1325 Km.

1091 e) The perturbations appear to bulge with depth, suggesting that subducted slabs undergo vertical  
1092 compression and folding? in which case, only the minimum widths of the original slabs can be  
1093 estimated.  
1094

1095 **Fig. 4 Overview tectonic sections of the study areas** (nomenclature “Almopias, Paikon and  
1096 Peonian” units after Kockel, 1979).

1097 a) western part of section shows obducted ophiolite, composed of serpentinite, peridotite, basalt,  
1098 gabbro and radiolarian chert, which was obducted together with tectonic mélangé over the Pelagonian  
1099 carbonate platform (Scherreiks 2000). The Elias formation has been interpreted as a relict of a supra-  
1100 subduction island arc complex (Scherreiks et al. 2014). Bauxite was deposited during the Callovian  
1101 (Scherreiks et al. 2016) (Table 1a 5 and 6). The eastern part of section a) shows overthrust,  
1102 supposed Vardar, Cretaceous platform carbonates and mylonitized ocean floor mélangé (devoid of  
1103 serpentinite). This nappe overlies the post-Eohellenic erosional unconformity of Upper Triassic  
1104 dolomite (Scherreiks and BouDagher-Fadel 2020a). Section b), shows the Vardar zone between the  
1105 Guevgueli ophiolite complex and Pelagonian ophiolite near Arnissa. Exposures of Pelagonia-derived  
1106 ophiolite s. str. occur in the western and central parts of the Almopias zone near Karydia and  
1107 Lyki/Klisochori; Serpentinite is not found in the units of the Paikon sub-zone (see also Fig. 6).  
1108

1109 **Fig. 5 Overview geologic map of Skopelos and Alonnisos in the Northern Sporades** (based on  
1110 Matarangas 1992; Kelepertsis 1974 and Scherreiks and BouDagher-Fadel 2020a), The Cretaceous  
1111 limestone formation of Alonnisos and Skopelos lies tectonically emplaced, together with a sheared  
1112 mélangé of metamorphic ocean-floor basalt and radiolarian chert, on top of the post-Eohellenic  
1113 erosional unconformity over Pelagonian Upper Jurassic limestone on Alonnisos and Upper Triassic  
1114 dolomite on Skopelos. It has been postulated that the tectonic emplacement took place during  
1115 Paleocene time as Pelagonia underthrust the Cretaceous forearc basin of the Vardar volcanic arc  
1116 (Scherreiks and BouDagher-Fadel 2020a).  
1117

1118 **Fig. 6 Geologic overview map of the Vardar and adjacent Pelagonian zone** (based on Mercier  
1119 and Vergely 1988 and 1984; Katrivanos et al. 2013; Georgiadis et al. 2016; and own field work). The  
1120 Pelagonian zone is in an underthrust position relative to the Cretaceous carbonate platform of the

1121 Vardar zone (Georgiadis et al. 2016) (B-B'). Imbricated ophiolite and Jurassic limestone are exposed  
1122 in a window extending from Margarita to Veria. Metamorphosed Pelagonian limestone is exposed in  
1123 the Gandach antiform of the Paikon sub-zone near Livadia. The tectonic section A-A' is shown in  
1124 Figure 4b. The formations between the Gandach marble and the Theodoraki limestone is a composite  
1125 mélange  
1126

### 1127 **Fig. 7 Chondrite-normalized REE and ternary discrimination diagrams**

1128 a. LREE enriched samples, probably IABs.  
1129 b. Flat REE and LREE depleted samples, most likely MORBs (see text).  
1130 c. Discrimination diagrams: Vardar-zone data (AFMs are also shown for Evvoia and the Northern  
1131 Sporades). The AFM from Perfit and others (1980) shows the plots of 1170 IABs (the dashed red line  
1132 area in the Vardar diagram, encompassing only a few of the Vardar meta-basalts).  
1133

### 1134 **Fig. 8 Composite tectono-stratigraphic synopsis:**

1135 a) Evvoia and the Northern Sporades were overthrust by the Eohellenic ophiolite which was  
1136 subsequently deeply eroded and transgressed by ~Cenomanian conglomerates. On the Northern  
1137 Sporades, the ophiolite and Lower Cretaceous had been removed by erosion before being  
1138 underthrust (D1-D3) beneath the Vardar-zone sheet during Paleocene time. b) Likewise, the Vardar  
1139 zone was underthrust by Pelagonia, which carried remnants of Eohellenic ophiolite and possibly  
1140 Cenomanian orthoconglomerates. c) schematic section through the Vardar ocean between Pelagonia  
1141 and Serbo-Macedonia indicating the widths (km) of oceanic lithosphere (see seismic tomography).  
1142 Legend: 1) Cretaceous and Paleocene carbonates. 2) mélange including Triassic radiolarite and  
1143 basalt, pyroclastic rocks, and carbonate slices. 3) Upper Jurassic (Pelagonian slices) and lower  
1144 Cretaceous Theodoraki carbonate slices. 4) Pelagonian ophiolite s. str. 5) Pelagonian Jurassic  
1145 carbonates 6) Pelagonian upper Triassic dolomite 7) Crystalline basement of Pelagonia. D1-D3  
1146 deformations (see text)  
1147

### 1148 **Fig. 9 Palaeogeography and time-laps cartoons**

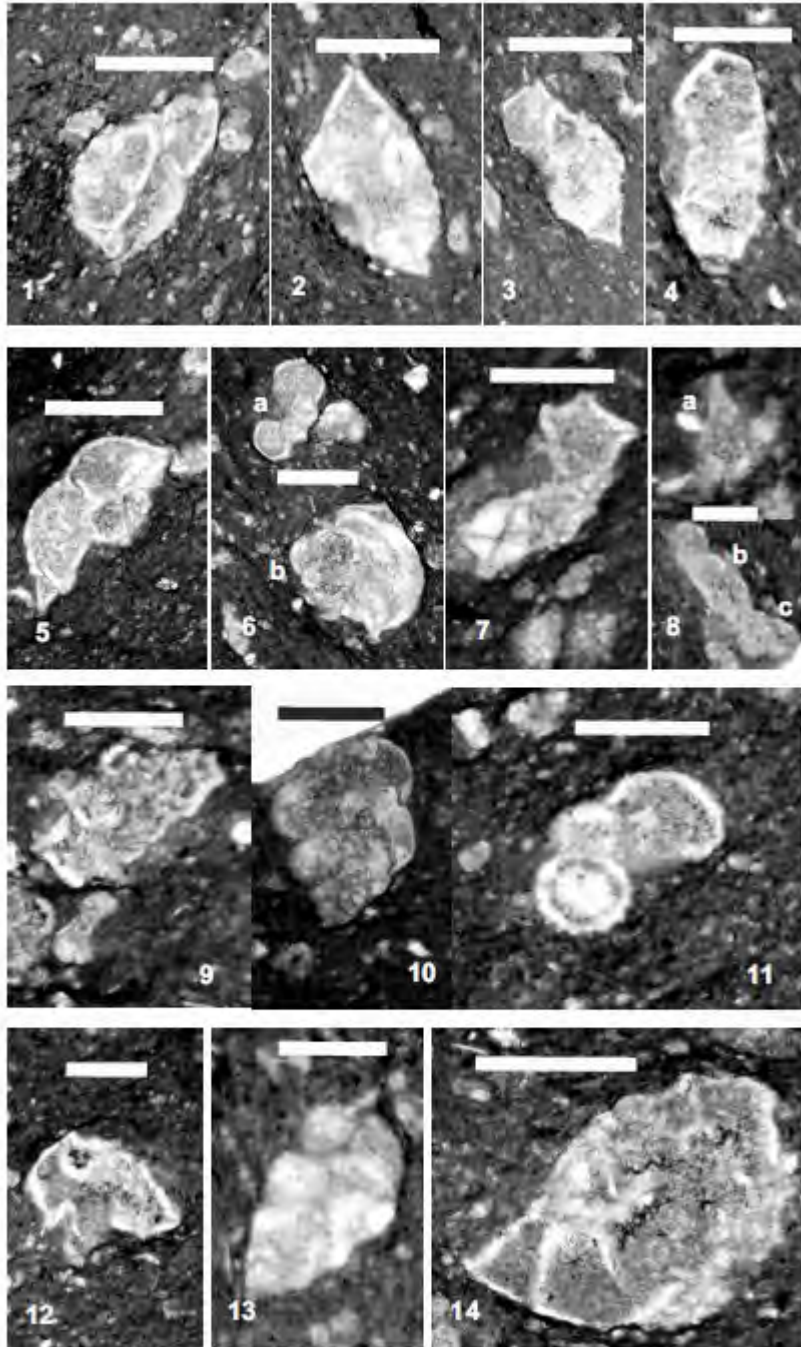
1149 a) The Vardar ocean was situated between two passive margins, continental Adria (including Korab-  
1150 Pelagonia) and Serbo-Macedonian Europe. Early Middle Jurassic intra-oceanic subduction led to the  
1151 demise of about 1200 km of Vardar lithosphere and to the obduction of about 200 km of the  
1152 Eohellenic ophiolite onto eastern Pelagonia. Subsequently, about 1700km of Vardar ocean  
1153 lithosphere subducted beneath the Paikon (east Vardar) island arc, followed by the crash of eastern  
1154 Pelagonia with the island arc, and finally (c) to the collision of Pelagonia with Serbo-Macedonia.  
1155 b) This time-laps cartoon shows the demise of the Vardar ocean in 7 stages. Pelagonia and Vardar  
1156 ocean lithosphere move NE toward, relatively autochthonous, Eurasia. Pelagonia and Vardar ocean  
1157 lithosphere move NE toward, relatively autochthonous, Eurasia. The Vardar ocean slabs are shown  
1158 as they reach their present position shown in Fig. 3c. It is important to note that the Earth's curvature  
1159 has been neglected in the graphic. This creates distortion in the lower mantle making it appear wider  
1160 than it should be.

#### 1161 *Time schedule of subduction*

1162 1) The Vardar ocean existed during Late Triassic time verified by radiolarians associated with pillow  
1163 basalt (Table 1a Carnian-Norian).  
1164 2) Intra-oceanic subduction was in progress around Toarcian to Aalenian time (180–170 Ma), based  
1165 on the metamorphic age of subduction-zone amphibolite mélange (Roddick et al. 1979; Spray and  
1166 Roddick 1980). Relative plate motions, however, had already changed from divergence to  
1167 convergence, during the Late Triassic, testified by the subsidence of the Rhaetian-Sinemurian  
1168 peritidal carbonate platform and change to the subtidal platform of Pliensbachian and Toarcian time  
1169 (Scherreiks et al. 2010) (Table 2a Rhaetian-Pliensbachian). Subduction of slab (x) continued through  
1170 the Middle Jurassic, verified by late Middle Jurassic radiolarians in ophiolite mélange in Evvoia  
1171 (Danelian and Robertson 2001; Scherreiks et al. 2014).  
1172 3) Platform uplift, erosion and bauxite deposition occurred during the Callovian (Meléndez et al. 2007;  
1173 Scherreiks et al. 2016), presumably due to the crash of the Eohellenic arc with the Pelagonian  
1174 platform (Callovian unconformity *ibid.*), causing upwarping of the carbonate platform. This stress  
1175 communicated across the east Vardar ocean causing subduction between east Vardar and Serbo-  
1176 Macedonia.



1177 4) As the Eohellenic ophiolite advanced, the carbonate platform subsided below the CCD during  
1178 Kimmeridgian-Berriasian time while back arc spreading was taking place in Guevgueli.  
1179 5) The final Eohellenic ophiolite emplacement takes place about Valanginian time. The west Vardar  
1180 slab x breaks off and sinks, the Pelagonian platform rises and deep (post-Eohellenic) erosion of the  
1181 Eohellenic nappe takes place. The Cretaceous carbonate platform evolves on top of volcanic debris  
1182 of the forearc basin and accretionary wedge. The east Vardar slab (y) continues to subduct.  
1183 6) Pelagonia crashes with the arc, underthrusts the Cretaceous carbonate platform and volcanic arc,  
1184 and the Guevgueli back arc basin.  
1185 7) Pelagonia crashes with Serbo-Macedonia while the Vardar slab breaks off and subsides.  
1186  
1187 c) The cartoon shows the final episode of Vardar ocean subduction. Pelagonia crashes and  
1188 underthrusts the arc and the Vardar slab breaks off. Pelagonia collides with Serbo-Macedonia which  
1189 initiates folding and renewed thrust faulting.  
1190  
1191  
1192  
1193  
1194



1195

1196

Plate 1

1197

1198 ?Scale bars: Figs 1 – 14

1199

1200 Fig. 1. *Contusotruncana fornicata* (Plummer).

1201 Fig. 2. *Globotruncanita stuarti* (De Lapparent).

1202 Fig. 3. *Globotruncana arca* (Cushman).

1203 Fig. 4. *Globotruncana linneiana* (d'Orbigny).

1204 Fig. 5. *Radotruncana subspinoso* (Pessagno).

1205 Fig. 6. a) *Rugoglobigerina hexacamerata* Brönnimann, b) *Radotruncana subspinoso* (Pessagno),

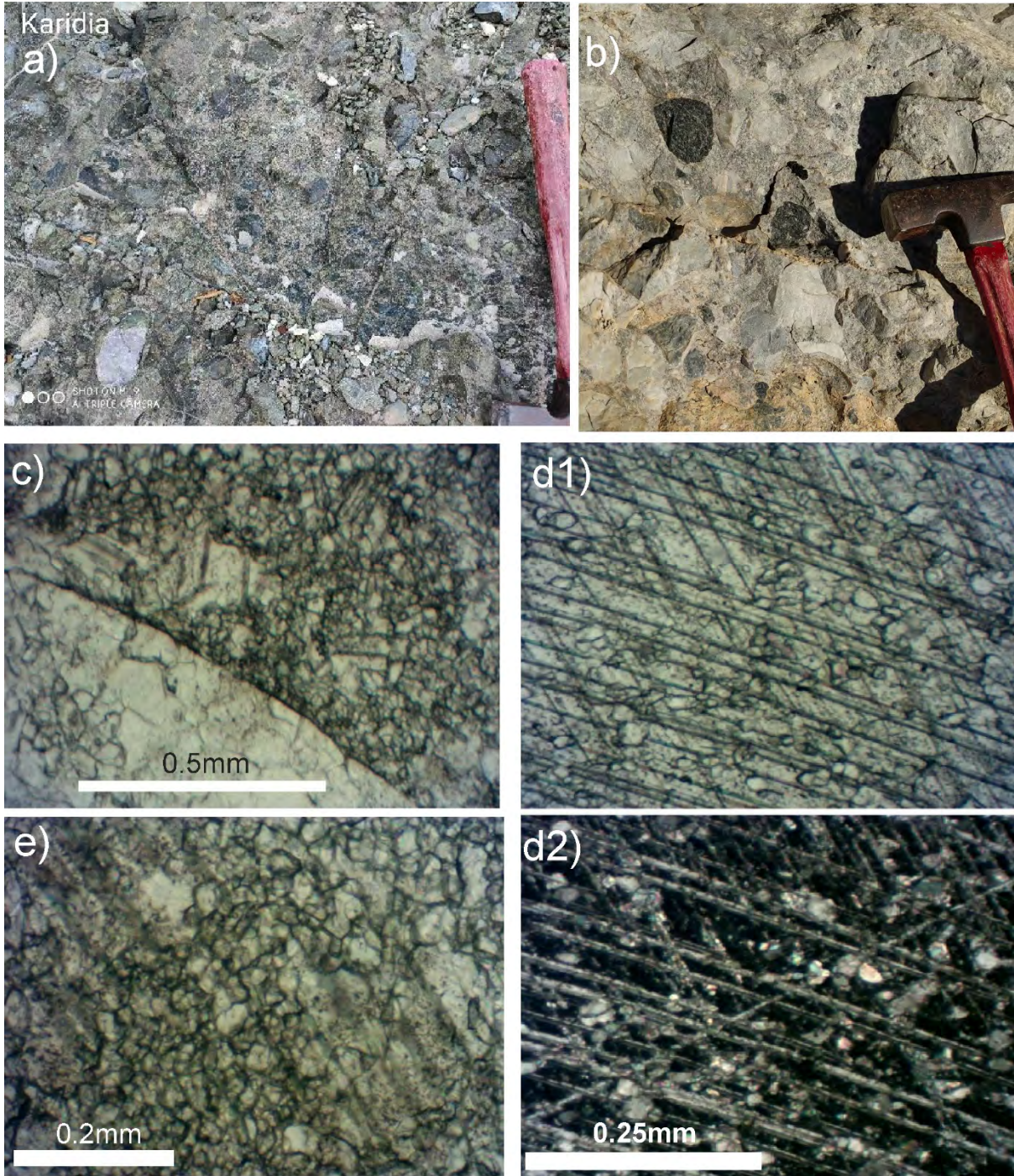
1206 Fig. 7. *Globotruncana aegyptiaca* Nakkady.

1207 Fig. 8. a) *Schackoina* sp., b) *Ventilabrella glabrata* (Cushman), c) *Rugoglobigerina hexacamerata*

1208 Brönnimann.



- 1209 Fig. 9. *Globo truncana lapparenti* Bolli.
- 1210 Fig. 10. *Heterohelix dentata* (Stenestad).
- 1211 Fig. 11. *Rugoglobigerina rugosa* (Plummer).
- 1212 Fig. 12. *Globo truncana rosetta* (Carsey).
- 1213 Fig. 13. *Heterohelix carinata* (Cushman).
- 1214 Fig. 14. *Globo truncanita atlantica* (Caron).
- 1215



- 1216
- 1217
- 1218
- 1219
- 1220
- 1221
- 1222 Plate 2a

- 1223 a. Field photo: breccio-conglomeratic ophiolite mélange in west Almopias, near Karydi
- 1224 b. Field photo: breccio-conglomeratic carbonate mélange in west Almopias near Nisi
- 1225 c. Photomicrograph: rounded grain of limestone and adjacent matrix of micro-breccia without cement.
- 1226 d1 and d2 Photomicrographs: neomorphic calcite (parallel and crossed nicols) in the matrix of 2b,
- 1227 showing palimpsest relic matrix grains and twinning planes.
- 1228 e-Photomicrograph: matrix of 2b showing initial palimpsest texture of growing neomorphic calcite in
- 1229 the matrix with recognisable twin planes

1230  
1231  
1232  
1233  
1234  
1235  
1236  
1237  
1238  
1239  
1240  
1241  
1242  
1243  
1244  
1245  
1246  
1247  
1248  
1249  
1250  
1251  
1252  
1253  
1254  
1255  
1256  
1257  
1258  
1259  
1260  
1261  
1262  
1263  
1264  
1265  
1266  
1267  
1268  
1269

**Table 1a** Biostratigraphic data, Evvoia and the Northern Sporades

<p><b>Table 1a biostratigraphy of Evvoia and Northern Sporades</b> (BouDagher-Fadel 2008; Scherreiks 2000; Scherreiks et al. 2010, 2014; Scherreiks and BouDagher-Fadel 2020a)</p>
<p><b>Pelagonian carbonate platform</b></p> <p><b>1. Rhaetian-Hettangian: peritidal/subtidal</b> ? <i>Aulotortus</i> sp., “<i>Aulotortus friedli</i>”, <i>Auloconus permodisoides</i>, <i>Grillina</i> sp. “<i>Vidalina</i>” <i>martana</i></p> <p><b>2. Sinemurian-Early Pliensbachian: shallow warm reef environment</b> <i>Siphovalvulina colomi</i>, <i>Siphovalvulina gibraltarensis</i>, <i>Duotaxis metula</i>, <i>Lituosepta recoarensis</i>, <i>Riyadhella praeregularis</i>. <i>Lituosepta compressa</i>, <i>Riyadhella praeregularis</i>, <i>Palaeodasycladus mediterraneus</i>, <i>Pseudocyclammina liasica</i>, <i>Lituosepta recoarensis</i></p> <p><b>3. Aalenian-Bathonian: shallow water environment</b> <i>Mesoendothyra croatica</i> Gusîc’</p> <p><b>4. Middle to Upper Jurassic: shallow water environment</b> BouDagher-Fadel 2008 <i>Neokillianina rahonensis</i></p>
<p><b>5. Bathonian-Callovian foraminifera suite: shallow warm reef environment This limestone occurs below the below the bauxite</b> <i>Pseudomarssonella bipartita</i>, <i>Redmondoides medius</i>, <i>Andersenolina elongata</i>, <i>Riyadhella</i> sp. <i>Ammobaculites</i> sp., <i>Trocholina</i> sp., <i>Palaeodasycladus</i> cf. <i>mediterraneus</i>, <i>Pseudopfenderina</i> sp., <i>Everticyclammina</i> sp., <i>Siphovalvulina</i> sp., <i>Riyadhoides</i> sp.</p> <p><b>6. Callovian-Oxfordian foraminifera suite on top of laterite: shallow reef environment</b> <i>Chablaisia</i> sp., <i>Septatrocholina banneri</i>, <i>Andersenolina elongata</i>, <i>Andersenolina</i> sp., <i>Palaeodasycladus</i> sp</p>
<p><b>7. Upper Jurassic shallow patch-reef environment</b> <i>Protopenneroplis striata</i>, <i>Parurgonina caeinensis</i>, <i>Thaumatoporella parvovesiculifera</i>, <i>Actinostromaria tokadiensis</i></p> <p><b>8. Late Berriasian-Early Valanginian: shallow reef environment</b> <i>Cladocoropsis mirabilis</i>, <i>Zergabriella embergeri</i></p>
<p><b>9. Late Cretaceous transgression in Evvoia, Maastrichtian: outer neritic environment</b> <i>Plummerita</i> aff. <i>hantkeninoides</i>, <i>Idalina</i> aff. <i>antiqua</i>, <i>Hippurites</i> sp., <i>Planorbulina cretae</i>: on a rudist clast (Campanian).</p>
<p><b>Cretaceous carbonate platform of the Northern Sporades</b></p> <p><b>10.1 Albian to Santonian: shallow reef environment</b> <i>Nezzazatinella picardi</i>, <i>Nezzazata convexa</i>, <i>Dicyclina schlumbergeri</i></p> <p><b>10.2 Late Santonian to Maastrichtian: reef/fore reef environment</b> <i>Rotorbinella</i> sp., <i>Orbitoides</i> sp., <i>Lithocodium</i> sp., <i>Lithocodium aggregatum</i>, rudists</p> <p><b>10.3 Early Paleocene: shallow reef environment</b> <i>Kathina</i> sp., <i>Daviesina</i> sp., <i>Lockhartia</i> sp</p>
<p><b>Radiolarians in Evvoia</b></p> <p><b>11. Ophiolite sheet:</b> Scherreiks et al. 2014, determined in co-operation with P. O. Baumgartner, Gingins and Schauner (Baumgartner et al. 1995).</p> <p><b>11.1 Carnian to Lower Norian:</b> <i>Annulotriassocampe</i> ? sp., <i>Castrum</i> ? sp., <i>Corum</i> ? sp., <i>Capnuchosphaera</i> cf. <i>crassa</i> <i>Capnuchosphaera</i> sp.</p> <p><b>11.2 Elias complex, Middle to Late Jurassic:</b> <i>Spongocapsula hooveri</i>, <i>Parvicingula dhimenaensis</i> s.l. <i>Transhuum brevicostatum</i>, <i>Protunuma</i> sp., <i>Sethocapsa</i> sp.</p>
<p><b>12. Ophiolite mélange</b> (Danelian and Robertson 2001; Gingins and Schauner 2005) <b>Middle Bathonian to Lower Callovian</b> <i>Parvicingula dhimenaensis</i> ssp., <i>Mirifusus fragilis</i> s.l., <i>Transhuum maxwelli</i> gr., <i>Tricolocapsa plicarum</i> s.l.</p>

1270  
1271  
1272  
1273  
1274  
1275  
1276  
1277  
1278  
1279  
1280



<p><b>Table 1b West and Central Almopias</b> After Mercier and Vergely 1988 Updated and additional age and palaeoenvironmental determinations (BouDagher-Fadel et al., 2015, 2018a, 2018b)</p>
<p><b>1. West Almopias</b></p> <p><b>1.1 Late Maastrichtian (Maastr, 2): inner neritic environment</b> Planktonic foraminifera <i>Abathomphalus mayaroensis</i>, <i>Globotruncana Stuarti</i>, <i>Contusotruncana contusa</i>, <i>Globotruncana arca</i> and <i>Globotruncana linneiana</i> and the larger benthic foraminifera <i>Orbitoides medius</i></p> <p><b>1.2 Santonian-early Campanian: shallow reef/intertidal environments.</b> The Hippuritidae, <i>Vaccinites atheniensis</i></p>
<p><b>2 Kato Grammatiko Pyrgi: Cenomanian (Cen. 1): foreereef/inner neritic environment.</b> Planktonic foraminifera <i>Rotalipora appenninica</i> and larger benthic foraminifera <i>Nezzazata simplex</i></p>
<p><b>3. Kerassia Campanian-Maastrichtian (Camp. 3b-Maast 2), : inner to outer neritic environment</b> <i>Globotruncana arca</i> [= <i>G. convexa</i>], <i>Globotruncanita</i> gr. <i>stuarti-stuartiformis</i></p>
<p><b>4 Kerassia – Nisi – Kedronas</b></p> <p><b>4.1 Campanian (3, 77.0-72.1Ma): Inner to outer neritic planktonic foraminifera in micritic wackestone:</b> <i>Radotruncana subspinosus</i>; <i>Heterohelix dentata</i>, <i>H. spp.</i>; <i>Globotruncana lapparenti</i>, <i>G. aegyptiaca</i>, <i>G. ventricosa</i>, <i>G. linneiana</i>, <i>G. rosetta</i>, <i>G. arca</i>; <i>Contusotruncana fornicata</i>; <i>Ventilabrella glabrata</i>; <i>Rugoglobigerina rugosa</i>, <i>R. hexacamerata</i>; <i>Globotruncanita atlantica</i>, <i>Gl. stuarti</i>, <i>Gl. sp.</i>; <i>Schackoia</i> sp.; <i>Globotruncanella</i> sp.; <i>Archaeoglobigerina blowi</i>.</p> <p><b>4.2 Aptian (Apt. 1-4a): reefal to inner neritic environment depositional depths of between 10 and 50m.</b> The presence of the larger benthic foraminifera <i>Palorbitolina discoidea</i> Gras (Barremian to Aptian), <i>Palorbitolina lenticularis</i>, indicate Aptian 1-4a age 125-115 Ma (see BouDagher-Fadel and Price, 2019).</p>
<p><b>5. Kerassia – Kedronas - Kato Grammatiko Campanian-Maastrichtian (Camp.3-Maast): reefal (rudist debris) to reworked in outer neritic</b> <i>Globotruncana arca</i>, <i>Globotruncanita stuarti</i>, <i>Globotruncana linneiana</i> [= <i>G. tricarinata</i>]</p> <p><b>5.1 Late Santonian (Sant.2): outer neritic</b> <i>Globotruncana lapparenti</i>, <i>Globotruncana arca</i> [= <i>G. convexa</i>], <i>Marginotruncana coronata</i>, <i>Sigalia deflaensis</i></p> <p><b>5.2 Early Santonian (Sant. 1): outer neritic</b> <i>Praeglobotruncana turbinata</i>, <i>Sigalitroncana sigali</i>, <i>Marginotruncana coronata</i>, <i>Globotruncana linneiana</i> <i>Globotruncana lapparenti</i>.</p>
<p><b>6 Jurassic exposures in the Kerassia-Nisi area (Pelagonian origin) Oxfordian-Early Cretaceous: low energy environment</b> <i>Stylosmilia</i> cf. <i>miehelini</i>, <i>Thecosmilia</i> cf. <i>langi</i>, <i>Cladocoropsis mirabilis</i>, <i>Dermosmilia</i> sp. and <i>Schizosmilia</i> cf. <i>rollieri</i> indicate a? Late Oxfordian-? Early Kimmeridgian age (in Sharp and Robertson 2006)</p>
<p><b>7. Central Almopias (Maragarita and Klissochori limestones on top of Jurassic mélange) with “conglomeratic” lenses</b></p> <p><b>7.1 Flamouria, (east of Edessa) Early Santonian: outer neritic</b> <i>Marginotruncana coronata</i>, <i>Globotruncana arca</i> [= <i>G.convexa</i>, <i>Marginotruncana marginata</i>. The shallow water Early Cretaceous. larger benthic foraminifera, <i>Orbitolina</i> sp. are reworked into the pelagic assemblages.</p>

**7.2 Messimeri (beneath Central Almopias mélange south of Edessa)** *Cladocoropsis* sp. Indicates Late Jurassic age and Pelagonian

1282  
1283  
1284  
1285  
1286  
1287  
1288  
1289  
1290  
1291  
1292  
1293

**Table 1b** Biostratigraphic data, west and central Almopias

<b>Table 1c East Almopias and Paikon</b> (after Mercier and Vergely 1984) updated age and environment (BouDagher-Fadel et al.,2015)
<b>1. Nea Zoi</b>
<b>1.1 Cenomanian (Cen. 3): outer neritic environment.</b> <i>Rotalipora cushmani</i> and <i>Praeglobotruncana stephani</i>
<b>1.2 Late Santonian-early Campanian (Sant.2-Camp.2): inner to outer neritic</b> <i>Globotruncanita elevata</i> , <i>Globotruncana convexa</i> , <i>Globotruncana arca</i> , <i>Orbitoides media</i>
<b>?2. Krania-Mavrolakkos Unit.</b> Radiolarian determinations (? P. De Wever & H. YiLing; in Sharp & Robertson 1998; 2006) ages ranging from Callovian to Early Cretaceous?
<b>3. Krania Unit: Mid-Oxfordian to Valanginian</b> Radiolarians reported by Stais (1994).
<b>4. Vryssi Unit and Nea Zoi Unit:</b> basalts are overlain by radiolarite of <b>Late Triassic</b> (Stais et al. 1990).
<b>Paikon</b>
<b>5- Theodoraki unit</b>
<b>5.1 Late Maastrichtian(Maast. 2-3): outer neritic</b> <i>Globotruncana linneiana</i> , <i>Contusotruncana contusa</i> , <i>Globotruncana arca</i>
<b>5.2 Maastrichtian (Maast. 2-3): outer neritic</b> <i>Globotruncana arca</i> [= <i>G. convexa</i> ], <i>Globotruncana linneiana</i> [= <i>G. tricarinata</i> ] <i>Globotruncana calciformis</i> , <i>Contusotruncana contusa</i> indicate late Maastrichtian age.
<b>5.3 Early Campanian (Camp 1-2): outer neritic</b> <i>Globotruncanita stuartiformis</i> indicates Campanian Santonian <i>Marginotruncana marginata</i> indicates an early Santonian age reworked into early Campanian assemblage.
<b>5.4 Early Cenomanian (Cen. 1): reef/inner neritic</b> <i>Orbitolina</i> gr. <i>Concava</i> , <i>Nezzazata</i> sp., <i>Cuneolina</i> sp, <i>Cyclolocolina</i> sp., <i>Pseudolituonella</i> sp. (see BouDagher-Fadel, 2018a)
<b>6. Griva-Khromni mélange</b> (from numerous researchers in Katrivanous et al. 2013).
<b>6.1 Aptian-Early Albian</b> <i>Mesorbitolina</i> sp., <i>Sabaudia minuta</i>
<b>6.2 Late Jurassic to Early Cretaceous</b> <i>Actinoporella</i> sp., <i>Pseudocyclamina</i> sp., <i>Cuneolina</i> sp., <i>Cladocoropsis mirabilis</i> , nerineid gastropods

1294  
1295  
1296

**Table 1c** Biostratigraphic data, east Almopias and Paikon

1297  
 1298  
 1299  
 1300  
 1301  
 1302  
 1303  
 1304  
 1305  
 1306

Analyte Symbol	SiO2	Al2O3	Fe2O3(T)	MnO	MgO	CaO	Na2O	K2O	TiO2	P2O5	LOI	Total	Sc	Be	V	Ba	Sr	Y	Zr	Cr	Co	Ni	Cu
Unit Symbol	%	%	%	%	%	%	%	%	%	%	%	%	ppm	ppm	ppm	ppm	ppm	ppm	ppm	ppm	ppm	ppm	ppm
Lower Limit	0.01	0.01	0.01	0.001	0.01	0.01	0.01	0.01	0.001	0.01	0.01	0.01	1	1	5	2	2	1	2	20	1	20	10
Method Code	FUS-ICP	FUS-ICP	FUS-ICP	FUS-ICP	FUS-ICP	FUS-ICP	FUS-ICP	FUS-ICP	FUS-ICP	FUS-ICP	GRAV	FUS-ICP	FUS-ICP	FUS-ICP	FUS-ICP	FUS-ICP	FUS-ICP	FUS-ICP	FUS-ICP	FUS-MS	FUS-MS	FUS-MS	FUS-MS
14	79.94	4.34	10.05	0.106	0.63	0.36	0.26	0.47	0.387	0.38	3.23	100.2	6	< 1	66	100	135	17	173	90	7	50	20
16	74.42	9.37	2.99	0.049	0.97	3.56	1.77	1.72	0.366	0.08	4.49	99.78	7	1	49	243	152	15	101	160	6	40	10
25	52.87	16.74	11.07	0.166	2.92	7.63	4.97	0.03	0.649	0.02	2.57	99.64	42	< 1	301	8	85	16	26	< 20	33	20	380
26	36.64	4.34	3.05	0.117	2.75	26.13	0.67	0.47	0.370	0.08	22.73	99.34	8	< 1	56	92	463	12	53	400	10	140	10
36	62.02	13.26	6.96	0.175	7.60	0.82	0.01	2.47	0.641	0.13	6.45	100.5	15	2	120	245	9	17	121	250	28	170	20
38	50.18	12.85	11.24	0.157	4.53	6.57	2.47	0.03	2.085	0.24	10.41	100.8	41	< 1	336	36	78	35	129	100	29	40	110
41	54.06	14.10	11.45	0.190	2.85	5.59	4.52	0.46	1.494	0.17	5.97	100.8	35	< 1	303	87	187	29	82	80	38	60	20
44	43.12	13.66	12.54	0.148	6.93	9.31	2.68	0.02	2.235	0.25	9.96	100.9	43	< 1	375	12	117	36	133	90	40	50	20

Analyte Symbol	Zn	Ga	Ge	As	Rb	Nb	Mo	Ag	In	Sn	Sb	Cs	La	Ce	Pr	Nd	Sm	Eu	Gd	Tb	Dy	Ho	Er
Unit Symbol	ppm	ppm	ppm	ppm	ppm	ppm	ppm	ppm	ppm	ppm	ppm	ppm	ppm	ppm	ppm	ppm	ppm	ppm	ppm	ppm	ppm	ppm	ppm
Lower Limit	30	1	1	5	2	1	2	0.5	0.2	1	0.5	0.5	0.1	0.1	0.05	0.1	0.1	0.05	0.1	0.1	0.1	0.1	0.1
14	80	7	1	195	10	6	3	0.6	< 0.2	1	9.5	< 0.5	19.3	29.1	4.14	16.3	3.5	1.65	2.9	0.5	2.8	0.6	1.5
16	30	10	< 1	< 5	62	4	< 2	< 0.5	< 0.2	1	1.4	2.0	15.7	30.6	3.76	14.7	3.1	0.89	2.5	0.4	2.6	0.6	1.6
25	70	15	2	< 5	< 2	< 1	< 2	< 0.5	< 0.2	< 1	0.7	< 0.5	1.5	3.6	0.55	2.9	1.2	0.42	1.8	0.4	2.8	0.7	2.1
26	90	4	< 1	6	15	2	< 2	< 0.5	< 0.2	1	0.5	1.4	6.8	13.9	1.72	6.8	1.6	0.49	1.8	0.3	1.9	0.4	1.1
36	80	15	2	< 5	92	10	< 2	< 0.5	< 0.2	2	< 0.5	3.0	19.3	35.5	4.79	18.5	4.3	1.06	3.6	0.5	4.0	0.8	2.2
38	500	15	< 1	10	< 2	3	< 2	< 0.5	< 0.2	1	0.5	< 0.5	4.1	11.9	2.00	11.5	4.1	0.97	5.8	1.1	7.2	1.5	4.4
41	50	15	1	8	4	< 1	< 2	< 0.5	< 0.2	< 1	1.1	1.8	4.2	12.0	2.00	10.5	3.8	1.29	4.9	0.9	5.6	1.2	3.6
44	100	17	1	< 5	< 2	3	< 2	< 0.5	< 0.2	1	0.7	< 0.5	5.7	15.5	2.66	14.1	4.5	1.63	6.4	1.2	7.6	1.6	4.4

Analyte Symbol	Tm	Yb	Lu	Hf	Ta	W	Tl	Pb	Bi	Th	U
14	0.25	1.6	0.32	3.5	0.4	1	0.3	78	< 0.4	4.7	2.0
16	0.24	1.5	0.26	2.4	0.4	< 1	0.3	11	< 0.4	5.4	1.3
25	0.35	2.4	0.42	0.9	< 0.1	< 1	< 0.1	< 5	< 0.4	0.6	0.3
26	0.16	1.1	0.17	1.1	0.2	< 1	< 0.1	< 5	< 0.4	1.4	0.5
36	0.31	2.1	0.32	2.9	0.7	1	0.4	< 5	< 0.4	8.2	1.6
38	0.66	4.3	0.67	3.3	0.2	1	< 0.1	263	< 0.4	0.3	0.5
41	0.53	3.5	0.55	2.3	< 0.1	2	< 0.1	< 5	< 0.4	0.4	0.4
44	0.64	4.1	0.60	3.2	0.2	< 1	< 0.1	< 5	< 0.4	0.3	0.9

Activation Laboratories Ltd. Report

FUS-ICP, FUS-MS: inductively coupled plasma mass spectrometry

1307  
 1308  
 1309  
 1310  
 1311

**Table 2a** major and trace elements for the Vardar zone (Fusion-Inductively Coupled Plasma Mass Spectrometry and Fusion Mass Spectrometry)

	SiO <sub>2</sub>	Al <sub>2</sub> O <sub>3</sub>	Fe <sub>2</sub> O <sub>3</sub>	MnO	MgO	CaO	Na <sub>2</sub> O	K <sub>2</sub> O	TiO <sub>2</sub>	P <sub>2</sub> O <sub>5</sub>	LOI	Total	Sc	Be	V	Cr	Co	Ni	Cu	Zn	Ga	Ge	As
1 Ev metabas	53.08	13.19	7.30	0.226	10.44	2.80	2.56	1.37	1.147	0.15	6.46	98.74	37	< 1	212	240	35	110	120	110	11	1	< 5
2 Ev serp Nikol	36.96	0.59	6.24	0.089	40.71	0.20	0.01	< 0.01	0.009	< 0.01	11.94	98.66	8	< 1	31	2440	112	2500	< 10	160	< 1	1	< 5
3 Ev perid Mour	42.13	1.08	8.91	0.130	45.25	1.32	0.03	0.01	0.010	< 0.01	-0.20	98.67	12	< 1	47	3040	112	2440	50	120	1	< 1	< 5
4 A1 basalt Agnati	55.42	16.16	9.92	0.111	5.43	1.03	6.11	0.03	0.611	0.04	4.83	99.71	46	< 1	338	< 20	34	20	160	90	15	< 1	18
5 A8 basalt Geor	61.36	16.66	7.44	0.077	4.11	0.32	1.25	2.95	0.815	0.11	4.43	99.55	18	2	137	210	17	110	30	110	21	2	8
6 S5 Bas Paloiki	47.33	15.64	12.26	0.160	7.43	5.78	3.64	0.28	1.959	0.22	5.11	99.81	41	< 1	361	240	42	110	50	120	16	1	< 5
Elias 01	70.94	13.60	5.32	0.121	1.63	0.11	0.42	3.83	0.599	0.06	3.85	100.5	14	2	124	320	16	19	116	70	20	50	70
Elias 02	72.35	11.81	4.72	0.087	1.54	0.14	0.31	3.62	0.499	0.05	3.29	98.4	12	2	106	271	14	12	94	60	18	70	70
Elias 03	53.48	16.03	11.26	0.112	2.55	6.23	6.53	0.13	1.174	0.26	2.61	100.4	38	< 1	333	43	94	18	73	830	31	220	30

	Rb	Sr	Y	Zr	Nb	Mo	Ag	In	Sn	Sb	Cs	Ba	La	Ce	Pr	Nd	Sm	Eu	Gd	Tb	Dy	Ho	Er
1 Ev metabas	31	76	20	80	8	< 2	< 0.5	< 0.2	< 1	< 0.5	1.4	86	10.4	27.4	2.97	12.6	3.3	0.94	3.9	0.7	4.0	0.8	2.4
2 Ev serp Nikol	< 2	2	< 1	< 2	< 1	< 2	< 0.5	< 0.2	< 1	< 0.5	< 0.5	3	< 0.1	< 0.1	< 0.05	< 0.1	< 0.1	< 0.05	< 0.1	< 0.1	< 0.1	< 0.1	< 0.1
3 Ev perid Mour	< 2	< 2	< 1	< 2	< 1	< 2	< 0.5	< 0.2	< 1	< 0.5	< 0.5	3	< 0.1	< 0.1	< 0.05	< 0.1	< 0.1	< 0.05	< 0.1	< 0.1	< 0.1	< 0.1	< 0.1
4 A1 basalt Agnati	< 2	103	17	28	< 1	< 2	< 0.5	< 0.2	< 1	< 0.5	0.6	22	1.9	5.2	0.66	3.2	1.3	0.30	2.0	0.4	2.6	0.6	1.9
5 A8 basalt Geor	130	59	23	162	12	< 2	0.5	< 0.2	3	< 0.5	3.6	462	23.0	49.1	5.54	20.8	4.5	0.97	4.1	0.7	4.3	0.8	2.4
6 S5 Bas Paloiki	7	32	38	153	4	< 2	< 0.5	< 0.2	1	0.5	< 0.5	23	5.4	15.6	2.72	14.3	4.6	1.44	6.7	1.1	7.2	1.5	4.3
Elias 01	70	19	< 1	< 5	137	9	< 2	< 0.5	< 0.2	2	< 0.5	5.5	36.3	78.0	8.04	30.2	5.3	1.04	4.1	0.6	3.9	0.8	2.4
Elias 02	70	14	< 1	< 5	109	8	< 2	< 0.5	< 0.2	2	1.4	4.2	28.1	55.4	6.28	23.3	3.6	0.60	2.1	0.4	2.2	0.5	1.5
Elias 03	100	9	1	6	2	15	< 2	< 0.5	< 0.2	< 1	1.7	< 0.5	9.7	19.1	2.57	11.0	2.6	0.90	2.7	0.5	2.7	0.6	1.7

	Tm	Yb	Lu	Hf	Ta	W	Tl	Pb	Bi	Th	U
1 Ev metabas	0.35	2.2	0.32	1.5	0.8	2	< 0.1	< 5	< 0.4	2.5	0.5
2 Ev serp Nikol	< 0.05	< 0.1	< 0.01	< 0.2	< 0.1	< 1	< 0.1	< 5	< 0.4	< 0.1	< 0.1
3 Ev perid Mour	< 0.05	< 0.1	< 0.01	< 0.2	< 0.1	< 1	< 0.1	7	< 0.4	< 0.1	< 0.1
4 A1 basalt Agnati	0.29	2.0	0.32	0.8	< 0.1	1	< 0.1	< 5	< 0.4	0.7	0.1
5 A8 basalt Geor	0.37	2.3	0.34	4.2	1.0	2	0.4	15	< 0.4	12.2	1.5
6 S5 Bas Paloiki	0.66	4.1	0.61	3.3	0.2	2	< 0.1	< 5	< 0.4	0.3	< 0.1
Elias 01	0.35	2.3	0.35	3.3	0.6	2	0.6	10	< 0.4	11.2	1.8
Elias 02	0.23	1.6	0.26	2.1	0.6	1	0.5	10	< 0.4	8.0	1.3
Elias 03	0.27	1.6	0.29	1.3	0.9	< 1	0.1	< 5	< 0.4	1.4	0.3

1312

1313 **Table 2b** major and trace elements for Evvoia and the Northern  
 1314 Sporades

1315 (same analytical information as in Table 2a)

1316